FINAL REPORT

SUBMITTED TO THE RADAR OPERATIONS CENTER
UNDER TERMS OF THE
RADAR OPERATIONS CENTER/OFFICE OF HYDROLOGIC
DEVELOPMENT MEMORANDUM OF UNDERSTANDING

June 2006 – May 2007

David Kitzmiller, Daniel Brewer, Feng Ding, Dennis
Miller, David Riley, and Shaorong Wu
Office of Hydrologic Development
NOAA National Weather Service
Silver Spring, Maryland

November 5, 2007

Table of Contents

Office of Hydrologic Development Report to the Radar Operations Center, 2007: Executive Summary

This report describes the results of evaluations of dual-polarization quantitative precipitation estimation and hydrometeor classification algorithms carried out by the Office of Hydrologic Development during the period June 2006-May 2007. The major findings can be summarized as follows:

Task 1.1 Part I: Evaluation of the NSSL Dual-Polarization Quantitative Precipitation Estimation (QPE) Algorithms – Echo Classification (EC) version 2007

This recently revised algorithm appears to improve upon both existing Z-R horizontal polarization algorithms and its immediate predecessor "Combined" algorithm, in terms of RMS error and percentage of 10-mm errors relative to collocated rain gauge reports. The EC algorithm also features less artificial noise than the Combined algorithm in fields of 1-hour rainfall; this feature was manifested as point values of zero rainfall in some precipitation areas characterized by hail or melting snow.

Task 1.1 Part II: Application of EC (Echo Classification) Rainfall Algorithm To NCAR S-pol Data from Florida During 1998

In the EC algorithm, the horizontal reflectivity / differential reflectivity rainrate sub-algorithm, R(Z,Zdr), is applied in most warm-season rainfall regimes, namely raindrops without contamination from melting snow or hail. This subalgorithm was evaluated over a sample of cases observed by the NCAR S-pol unit over the central Florida peninsula in summer, 1998. Though the results did not indicate that the dual-polarization rainfall estimates were clearly superior to horizontal-polarization estimates in this regime, the dual-polarization algorithm still yielded realistic and reliable results. It is possible that further calibration of the R(Z,Zdr) algorithm parameters based on subtropical data would give appreciable improvement over the current operational algorithm.

Task 1.2: Potential Applications Of NSSL Dual-Polarization Hydrometeor Classifier Algorithm (HCA) As A Precipitation/No Precipitation Filter

Some events with a common operational problem, namely WSR-88D estimates from a single radar featuring both precipitation and return from migrating birds, were examined through observations from both the KOUN dual-polarization and KTLX WSR-88D units. The data applied here involved an earlier version of the Hydrometeor Classification Algorithm (HCA) than is presently available. However a comparison of precipitation estimates from both radar units showed the ability of the HCA to detect and remove large regions of apparent light precipitation due to biota, while retaining real precipitation. The results were confirmed with rain gauge reports.

Task 1.1 Part I: Evaluation of the NSSL Dual-Polarization Quantitative Precipitation Estimation (QPE) Algorithms – Echo Classification (EC) version 2007

Introduction

Evaluations of the dual-polarization QPE algorithms proposed for operational implementation were carried out in order to identify potential problems and to develop guidance for end users who are expected to adapt their operations to use dual-polarization estimates in place of current ones. Both subjective evaluations of visual imagery and numerical comparisons of point values with coincident rain gauge estimates have been prepared.

As reported by NSSL researchers Ryzhkov and Krause in February 2007 (presentations to OHD, ROC, and NEXRAD SREC), the NSSL proposed QPE algorithm continues to evolve. A large sample of point values from the most recent version, referred to as the Echo Classification (EC) version, was made available to OHD and we have carried out an initial evaluation of 1-h rainfall estimates from EC and compared them to the output of Combined, the convective Z-R relationship applied to horizontal polarization reflectivity data, and collocated rain gauge reports from the Oklahoma Mesonet. All dual-polarization radar data were collected from the KOUN experimental unit in Norman. This collection of radar and gauge estimates, ~15,800 cases, is hereafter referred to as the "statistical" dataset.

In June 2007, NSSL staff provided another sample of 100 hours' gridded EC and Z-R estimates over 6 calendar days in 2004-2005. We collated the radar estimates from these 1-h, 2-km mesh-length grids with simultaneous estimates from the KTLX (Twin Lakes) WSR-88D unit, and rain gauge reports from the Oklahoma Mesonet. Mesonet observations from 119 sites were obtained from the Oklahoma Climate Survey's web site. This data collection of ~8,400 cases is hereafter referred to as the "gridded" dataset.

Both the statistical and gridded collections of gauge/radar pairs were augmented with operational estimates from KTLX primarily as a reference for general skill level. Since the KTLX unit undergoes routine operational calibration, it is possible that its overall calibration is superior to that of KOUN, which served as an engineering testbed during much of the study period to date. Based on comparisons between Z-R and EC estimates from the KOUN unit, we can still expect improvements over current horizontal-polarization Z-R estimates following the dual-polarization upgrade to operational WSR-88D units.

A further subjective analysis of the gridded data in imagery format is included here, to demonstrate the EC algorithm's basic consistency with horizontal polarization estimates and to determine if certain artifacts that appeared in the earlier Combined dual-pol algorithm had been mitigated.

1.1 Analysis of gauge/radar estimate pairs from statistical development and validation dataset, 2002-2005

An evaluation of the approximately 16,000 radar/gauge report pairs in the dataset provided by NSSL indicates that the EC algorithm features lower RMS error than the Z-R algorithm, and that

the tendency of the Z-R algorithm to be biased high in the higher range of values is greatly mitigated; these properties were reported by Ryzhkov et al. (2007). These improvements are detected at all ranges within the 235-km range umbrella but are most noticeable in the inner 150-km umbrella, the range zone in which most operational estimates are used. We carried out slightly different analyses to determine potential impacts on hydrologic operations and flash flood monitoring.

Specifically, we examined the spectrum of 1-h rainfall values from gauges, EC, and Z-R estimates from both KOUN and KTLX, to determine if the range of values is similar. This analysis does not incorporate any consideration of correlation between the radar and gauge estimates. We also compared the gauge correlation of the EC, Z-R, and operational Digital Precipitation Array (DPA) algorithms when mean-field bias correction was applied, under two assumptions about the density of an operational gauge network. While the NSSL documentation clearly indicates that EC improves on the Z-R method, the operational practice of real-time gauge/radar mean-field bias correction alone yields appreciable improvement in some verification statistics. Therefore, we wished to verify that the dual-polarization approach still yields improvements over horizontal-polarization when some real-time gauge data is available to correct the Z-R estimates.

1.2 Statistical evaluation of EC and Z-R algorithms, relative to rain gauge observations

Our evaluation includes statistics and data stratification not shown in the course of the NSSL presentations described earlier, and a comparison between EC and operational Digital Precipitation Array (DPA) products from the nearby KTLX WSR-88D unit. As noted below, we cannot expect the overall performance of the KOUN unit, a research and test platform whose electronics were modified several times during the study period, to match that of the operational KTLX radar. However, we found that the quality of the Z-R estimates from KOUN was comparable to the KTLX estimates, in terms of correlation with matched sets of rain gauge reports.

A known problem with current short-period radar estimates based on horizontal polarization and a power-law Z-R relationship is that, after correction for bias over the long term, the lowest radar values (typically < 5 mm) are underestimates while the higher amounts (> 10 mm) are generally overestimates (see for example Ciach and Krajewski 2005). Expected values of rain gauge reports over several sub ranges of radar-estimated values are shown in Fig. 1-1, which is based on all radar-gauge pairs in which either the gauge, EC, or Z-R indicated at least 0.25 mm of precipitation. Each plotted point in the figure represents at least 200 gauge/radar pairs, stratified by the radar-estimated value. The Z-R estimates from KOUN appear be biased high for values ≥ 5 mm h^{-1}, while the EC values show only a slight tendency to overestimate the higher values

This is partly an effect of selective stratification. We found that the gauge and all radar estimates have approximately the same form of statistical distribution, as shown in Fig. 1-2a. Following long-term bias correction (multiplying all radar estimates by the ratio of gauge to radar precipitation within the entire sample), differences among the various rainrate spectra become still smaller, as shown in Fig. 1-2b. These results suggest that the apparent distortion in Fig. 1-1

is due in part to sampling differences between radar and gauge platforms, and/or misrepresentation of the drop-size distribution in uncommonly heavy rainfall situations.

The EC output features a much closer general fit to the gauge amount distribution through all ranges (Fig 1-1). It should be noted that the Z-R and EC have approximately the same correlation with the gauge amounts, and thus the same information content, but the better overall calibration of the EC has some important advantages from a hydrologic viewpoint.

1.3 Radar algorithm performance after real-time mean-field bias correction – statistical dataset

Ryzhkov et al. (2007) presented RMS error statistics indicating that EC represented an improvement over Z-R estimates when all gauge-radar pair data were pooled for several events over several years. We repeated this analysis under a different set of assumptions, and also evaluated algorithm performance in terms of large errors, namely the fraction of critical rain events where gauge or radar indicated ≥ 10 mm of rainfall in 1 hour, and the absolute radar error was ≥ 10 mm.

The initial analysis did not account for possible advantages gained by real-time mean-field bias (MFB; Seo et al. 1999) correction, either for the Z-R or EC estimates. We applied such corrections, estimating the bias from the current hour's data and when necessary that from previous hours, with data more that 3 hours old receiving a lower statistical weight. A minimum of 10 gauge radar pairs was considered adequate for bias estimation, though more than 10 pairs were used when the estimate incorporated data older than 3 hours.

Because the density of the available gauge network in many places is lower than that of Oklahoma, and the reporting latency of individual gauge sites is often several hours, the gauge reports were randomly thinned to 33% and 25% of the maximum number available. Error statistics are based on data from all gauge locations. Note that the bias correction factor is based on the entire collection of available gauges, and thus the bias information does not contribute spatial detail. Though some of the same gauge information is used in both bias correction and verification, our purpose is to compare radar algorithms, and therefore the application of gauge data has little effect on the final result.

We stratified the error statistics according to two range criteria. These were < 150 km, the range from which most operational radar estimates are taken, because of network coverage overlap, and the generally accepted maximum effective detection range of 230 km. A few field offices are obliged to monitor parts of their warning areas with long-range estimates only, where the radar network is less dense or where beam blockages or other factors degrade detection from radars that are physically closer.

Within the 150 km range band (results summarized in Figure 1-3), where 6900 cases met the minimum precipitation criterion, we found the RMS errors for EC and Z-R with no MFB correction were 2 and 3.5 mm, respectively. As a reference, the error for the KTLX DPA estimates was 2.7 mm (Fig. 1-3a). Applying MFB corrections with 33% of the available gauge

reports substantially reduced the EC, Z-R, and DPA errors to 1.8, 2, and 2 mm, respectively. Corrections based on 25% of the gauges yield RMS errors of 1.8, 2, and 2.1 mm respectively.

For many operations, heavier amounts are more critical to operational decisions. To examine algorithm performance in such events, we calculated another error statistic for the cases in which at least one of the three estimates (gauge, EC, or Z-R) was ≥ 10 mm. Though this amount is not usually heavy enough to cause flash flooding, it does indicate rain rates high enough to restrict visibility and have significant impacts on some activities such as ground transportation. Here, the statistic is the percentage of cases in which the absolute radar-gauge error is ≥ 10 mm, a rather substantial amount but not uncommon in Z-R estimates.

As shown in Figure 1-3b, the percentage of radar estimates with large errors, with no real-time MFB correction, ranges from 31% for the original Z-R estimates to 20% for KTLX DPA estimates to near 10% for EC. Application of MFB correction led to considerable reduction in the error percentage for the Z-R estimates and smaller but appreciable reduction in errors from the EC estimates (to near 11% and 8% for either 25% or 33% of the gauge network being used in MFB correction).

Thus it appears that gauge data alone, applied only through MFB correction, can substantially reduce the error in Z-R estimates toward that of the EC estimates, though the EC estimates themselves could benefit from MFB correction. It must be noted that in many radar umbrellas, even less rain gauge data is reliably available, or the gauge network is very unevenly distributed. For such field offices, the use of dual-polarization algorithms will still be critical to reducing uncertainty in real-time rainfall estimates.

Very similar results were obtained when this analysis was repeated for the entire 230-km radar umbrella (Figure 1-4). Again, the KOUN Z-R and KTLX DPA estimates were substantially improved by the incorporation of real-time gauge data, while EC showed smaller but appreciable improvements. The decreased ability of the EC algorithm to improve Z-R is likely due to the increased influence of range effects, particularly beam spreading and vertical profiles in hydrometeor types and reflectivity patterns. The present EC algorithm does incorporate some compensation for reflectivity profile effects such as radar detection of dry or melting snow; a more permanent improvement must involve some form of real-time reflectivity profile correction.

1.4 Conclusions based on the 2002-2005 statistical dataset

The EC estimates evaluated were generally lower than the amounts estimated by the standard Z-R relation. EC shows markedly lower estimates versus Combined in the convective cores on the outer ranges of the radar. The EC algorithm mitigated areas of apparent bright band enhancement at mid ranges during the cool season. It also eliminated much of the "noise" and "zero dropouts" in the Combined estimates. There is a reduction of precipitation estimates close to the center of the radar range on all the output from EC. This is likely due to excessive clutter suppression on the lowest scan. The inclusion of data from higher tilts in future updates to the EC algorithm should mitigate this effect.

The EC dual-polarization algorithm improves on Z-R estimates in terms of RMS error and number of large errors, relative to 1-h gauge reports, even when substantial amounts of coincident rain gauge information is used to bias-correct the Z-R estimates. In areas with dense gauge coverage, there is an advantage to incorporating MFB correction to the EC estimates. The addition of the dual-polarization data is roughly equivalent to that of having a dense network of rain gauges available for bias correction of current Z-R estimates. Note that the Oklahoma Mesonet, with 92 gauge sites within the KOUN 250-km umbrella, is exceptionally dense when compared with most other real-time reporting networks.

It should be noted that many cases in this statistical dataset were part of the sample used to develop and calibrate the EC algorithm set (Giangrande and Ryzhkov, personal communication). Therefore the superior performance of EC relative to the Z-R algorithm is to some extent assured. However, we were able to confirm that EC yielded a closer approximation to collocated rain gauge measurements within another data sample containing independent observations, as described below.

1.5 Analysis of gridded dataset, including 6 study days 2003-2005

A sample of gridded data containing ~110 hours' precipitation estimates was selected by OHD and provided by NSSL, as follows:

14 May 2003:	convective rainfall
11 June 2003:	convective rainfall
21 April 2004:	convective rainfall with some hail
3 June 2004:	convective and stratiform rainfall
9-10 June 2004:	primarily convective rainfall
15 November 2004:	stratiform rain with bright-band enhancement
6 February 2005:	stratiform rain with bright-band enhancement; snow possible at a few locations

Several hours in which there were more than 11 minutes of missing volume scan data were removed. A total of 95 hours of data remained in which both EC and Z-R estimates, and DPA estimates from KTLX, were available.

One preliminary analysis was made to estimate the effect of changing the data format from azimuth-range to gridded (2-km rectangular mesh). A total of 15 hours of data from 3 of the days (14 May; 11 June; 15 November) were available from both the statistical and gridded datasets; there were 1305 gauge/radar pairs within this sample. The two sets of radar estimates, and rain gauge data, were collated and the respective correlation statistics compared.

We found that the correlation statistics overall were similar: the rank correlation between radar and gauge was 0.85 and 0.87 from the gridded and statistical datasets, respectively, and the RMS errors were 1.6 and 1.8 mm. There were some apparently random differences between the gridded and azimuth range rainfall estimates, as might be expected given the differing areas for spatial averaging. A final dataset was created by finding the gridded rainfall value closest to the azimuth-range value specified for the given gauge location. The rank correlation and RMS error

for this set of cases was 0.88 and 1.6 mm, respectively. We concluded that there were only minor differences in correlation statistics introduced by the differing grid resolutions.

Another preliminary analysis was made to confirm as far as possible that the change from the Combined to the EC algorithms lead to consistent improvement in a statistical sense. Data from 95 hours on which data from both the EC and Combined algorithms (the latter processed in 2006) were collated with gauge data, yielding 8936 cases. The rank correlations for the EC and Combined algorithms were 0.69 and 0.71, respectively; the RMS errors were 1.2 mm and 1.4 mm respectively. Within the subset of 3416 cases where some rainfall was observed by either gauge or radar, the EC and Combined rank correlations were 0.52 and 0.49, while the RMS errors were 1.9 and 2.3 mm. Thus the Combined algorithm appeared to yield more cases with large errors than did the EC.

Given these statistics and general improvement in the spatial continuity and physical consistency of the rainfall fields as shown in imagery (following section), we believe the improvements yielded by the EC algorithm are operationally significant and will be of benefit to end users.

1.6 Radar algorithm performance after real-time mean-field bias correction –gridded dataset

We repeated the analysis of the effects of real-time MFB correction, described in a previous section. For these experiments, approximately 8400 cases were available within the KOUN 250-km umbrella and 4700 within the 150-km inner umbrella.

While the KOUN Z-R and KTLX DPA estimates were still improved by MFB correction, the degree of improvement was less than that seen in the statistical dataset; the EC estimates were not consistently improved. As shown in Figs. 1-5 and 1-6, the use of fewer gauges for bias correction sometimes resulted in slightly lower RMS errors and/or a lower percentage of 10-mm errors. This could be due to chance, given that this collection of cases was chosen more for rainfall intensity and range of precipitation types than for coverage by rainfall. Moreover the time series was necessarily fragmented, with the case days being separated by weeks or months, making bias correction with older data less meaningful. In operational practice such large temporal gaps will be experienced only rarely.

We still found that EC consistently improved on the KOUN Z-R estimates, even after application of MFB correction, as was found in the tests on the larger statistical dataset. Thus it is reasonable to expect continued improvement

1.7 Subjective visual analysis of samples cases from 2003-2005

Sample 1-h rainfall estimate fields from each of the study events are shown in Figs. 1-1 to 1-9. The events can be characterized as follows:

21 April 2004:	convective rainfall with some hail (Figs. 1-7, 1-8)
3 June 2004:	convective and stratiform rainfall (Fig. 1-9)
9-10 June 2004:	primarily convective rainfall (Figs. 1-10, 1-11)
15 November 2004:	stratiform rain with bright-band enhancement (Figs. 1-12, 1-13)

6 February 2005: stratiform rain with bright-band enhancement (Figs. 1-14, 1-15)

The subjective analysis described below includes output from 3 algorithms and two different radar units. Estimates from the KOUN experiment unit include the "Combined" algorithm described in our last report, output from the newer EC algorithm, and estimates from the convective Z-R algorithm. For purposes of comparison, output from the operational KTLX WSR-88D unit's Z-R algorithm is also shown (Figs. 1-8, 1-11, 1-13, 1-15). Figures 1-7 to 1-11 show the Combined algorithm estimates (labeled "a" in each figure), EC estimates (labeled "b") and Z-R estimates based on the convective relationship $Z=300R^{1.4}$ (labeled "c").

The EC estimates appear to show marked improvement over the Combined in terms of spatial continuity; there are fewer data holes in the 2-km analysis grid and fewer unrealistic range-dependent features that were introduced by the Combined specification that all rainfall estimates beyond 200 km were derived from the Z-R algorthm .

The EC estimates associated with convective precipitation (Figs. 1-7 to 1-11) are generally lower than the highest amounts indicated by the Z-R estimates. This is likely a positive attribute of the EC algorithm in mitigating likely overestimates due to the presence of hail. EC is slightly lower then Combined estimates in these hail cores.

EC shows markedly lower estimates versus Combined in the convective cores on the outer ranges of Fig. 1-7. This is a positive effect again mitigating likely hail contamination and primarily due to Combined defaulting to the horizontal Z-R relationship beyond 200 km while the choice between rainfall relations is based on the results of precipitation classification in EC. EC removed the residual "noisiness" and "holes" from the Combined estimates.

For both cool season events (Figs. 1-13 to 1-15) there is a suggestion of bright-band enhancement. The EC algorithm mitigated areas of apparent bright band enhancement at mid ranges of the radar umbrella. It also eliminated much of the "noise" and "dropouts" in the Combined estimates.

There is a reduction of precipitation estimates close to the center of the radar range on all the output from EC, most noticeable on Figs. 1-9, 1-10, and 1-11. This is likely due to excessive clutter suppression on the lowest scan. The inclusion of data from higher tilts in future updates to the EC algorithm should mitigate this effect.

Acknowledgements

We appreciate the assistance in data acquisition and subject review provided by Alexander Ryzhkov, John Krause, and Scott Giangrande.

References

Ciach, G., and W. Krajewski, 2005: Towards Probabilistic Quantitative Precipitation WSR-88D Algorithms: Data Analysis and Development of Ensemble Generator Model: Phase 4. Report to Office of Hydrologic Development, National Weather Service, NOAA, 206 pp.

[Available from: http://www.nws.noaa.gov/oh/hrl/papers/wsr88d/PQPE-FinalReport.pdf]

Ryzhkov, A., 2007: Graphical presentation to NEXRAD SREC, March 2007 [available from author].

Seo, D.-J., J. P. Breidenbach, and E. R. Johnson,1999: Real-time estimation of meanfield bias in radar rainfall data. *J. Hydrology*, **223**, 131-147.

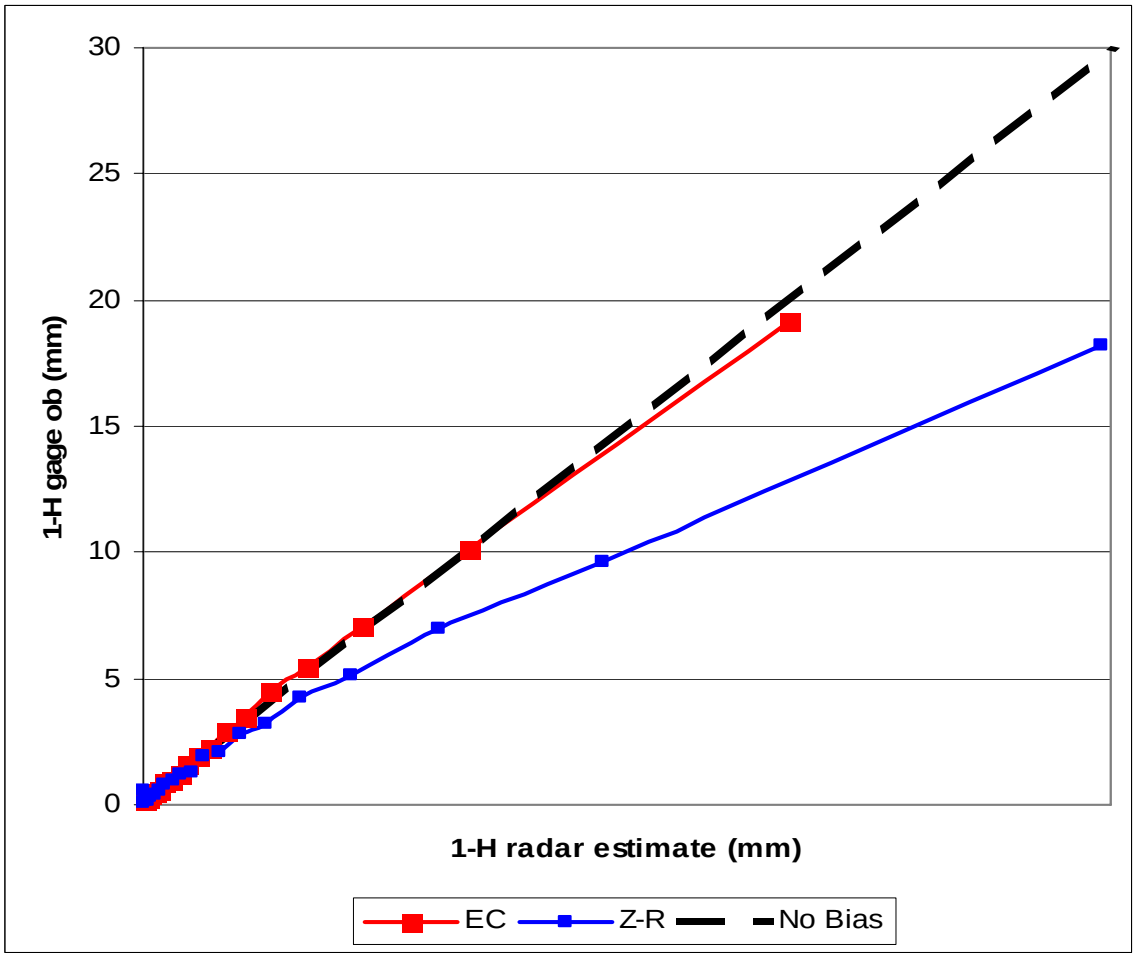

Figure 1-1. Expected 1-h rain gauge amount as a function of radar-estimated values, from 2002-2005 NSSL dataset. Rain gauge reports are from Oklahoma Mesonet sites, At ranges 25-230 km from the KOUN radar unit. Each plotted point on the trace represents approximately 250-350 gauge-radar pairs.

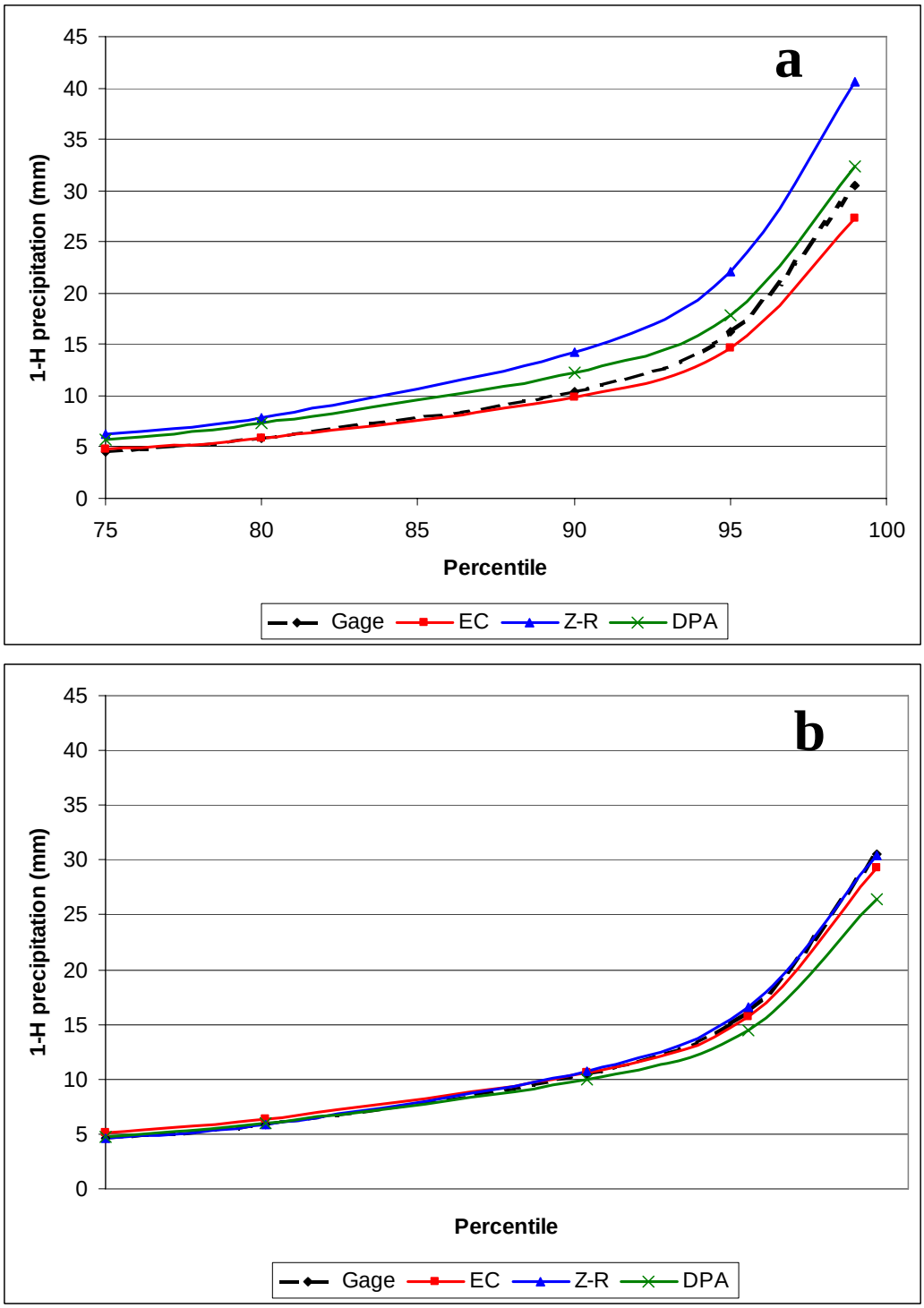

Figure 1-2. 1-h rainfall distribution by percentile, mm, from 2002-2005 NSSL dataset. Rain gauge reports are from the Oklahoma mesonet, ranges 25-230 km from the KOUN radar unit. EC and Z-R are from KOUN; DPA values are from WSR-88D KTLX. Percentiles are within the subset of cases in which precipitation > 0.25 mm. Original radar values are evaluated in (a), values after long-term bias correction in (b).

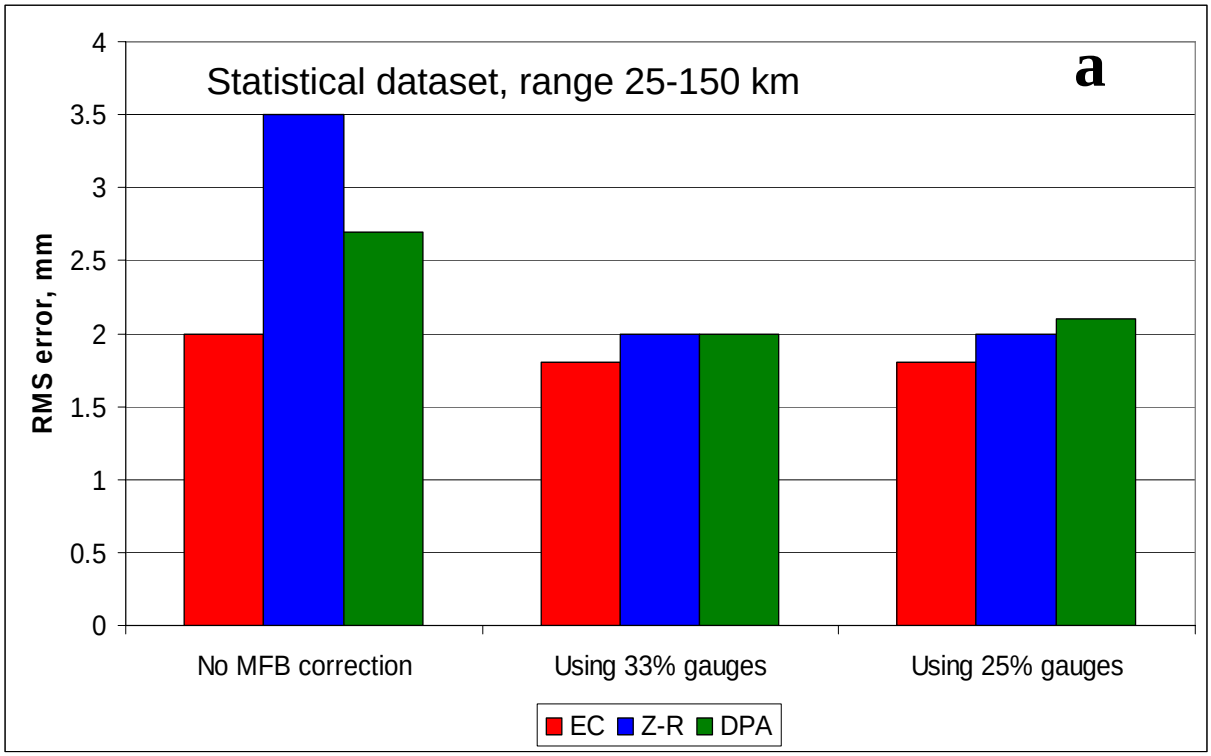

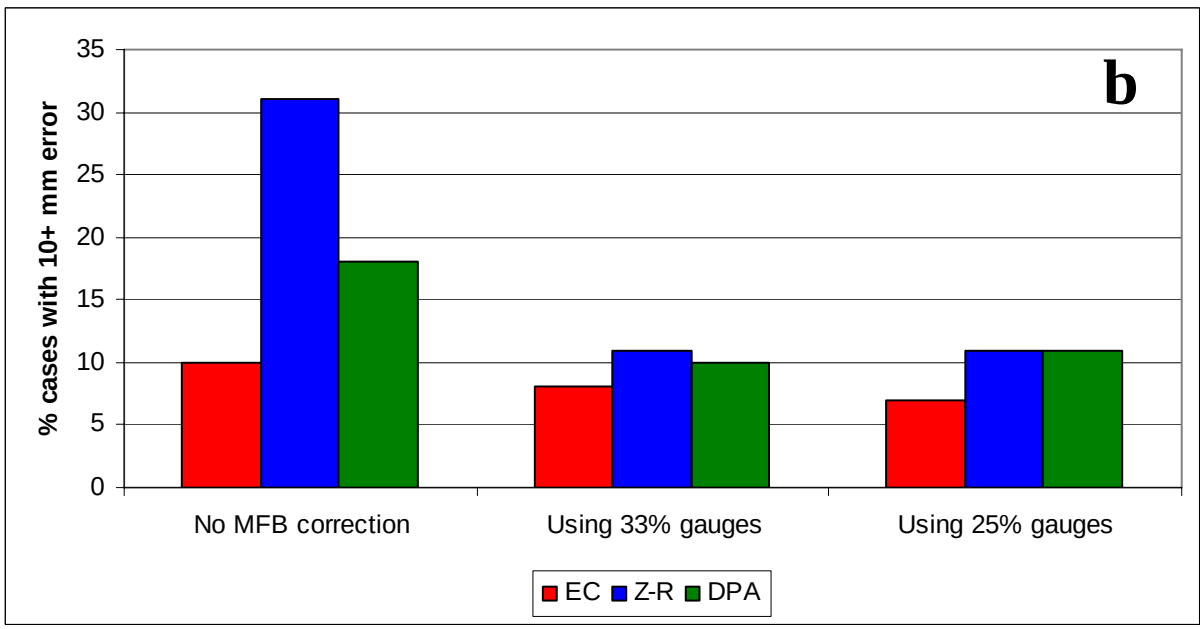

Figure 1-3. Effects of real-time gauge/radar mean-field bias bias correction on (a) root mean squared error and (b) percentage of heavy precipitation cases with radar-gauge errors of 10 mm or more. All data are for Oklahoma Mesonet gauge locations between 25 and 150 km from the KOUN radar unit. RMS errors are for 6901 cases within the statistical gauge/radar dataset supplied by NSSL; percent cases with 10-mm errors are from 592 cases in which gauge or a radar estimate indicated > 10 mm rainfall.

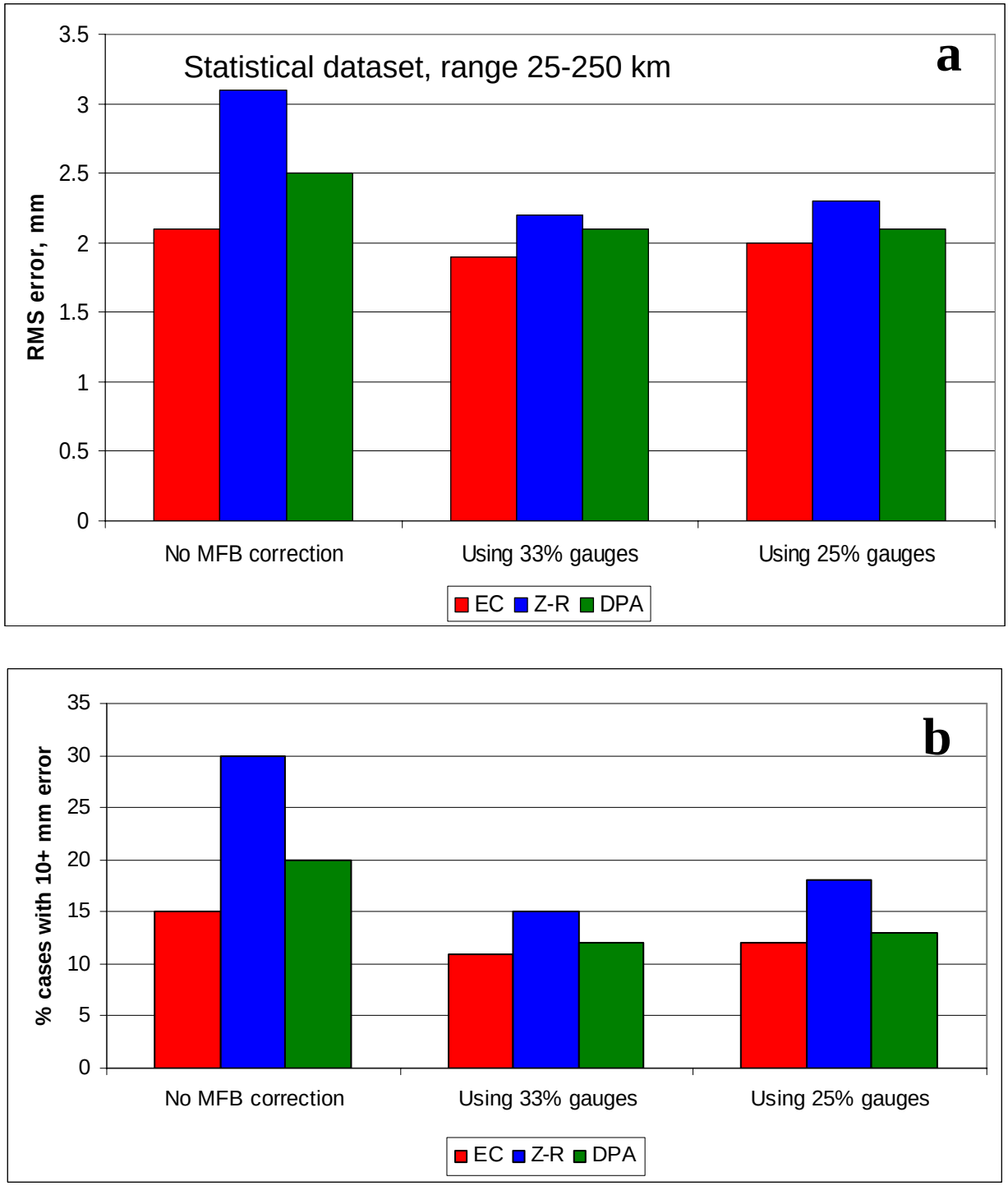

Figure 1-4. As in Fig. 1-3, except gauge locations are between 25 and 250 km from the KOUN radar. RMS errors are for 13213 cases; percent cases with 10-mm errors are from 953 cases in which gauge or a radar estimate indicated > 10 mm rainfall

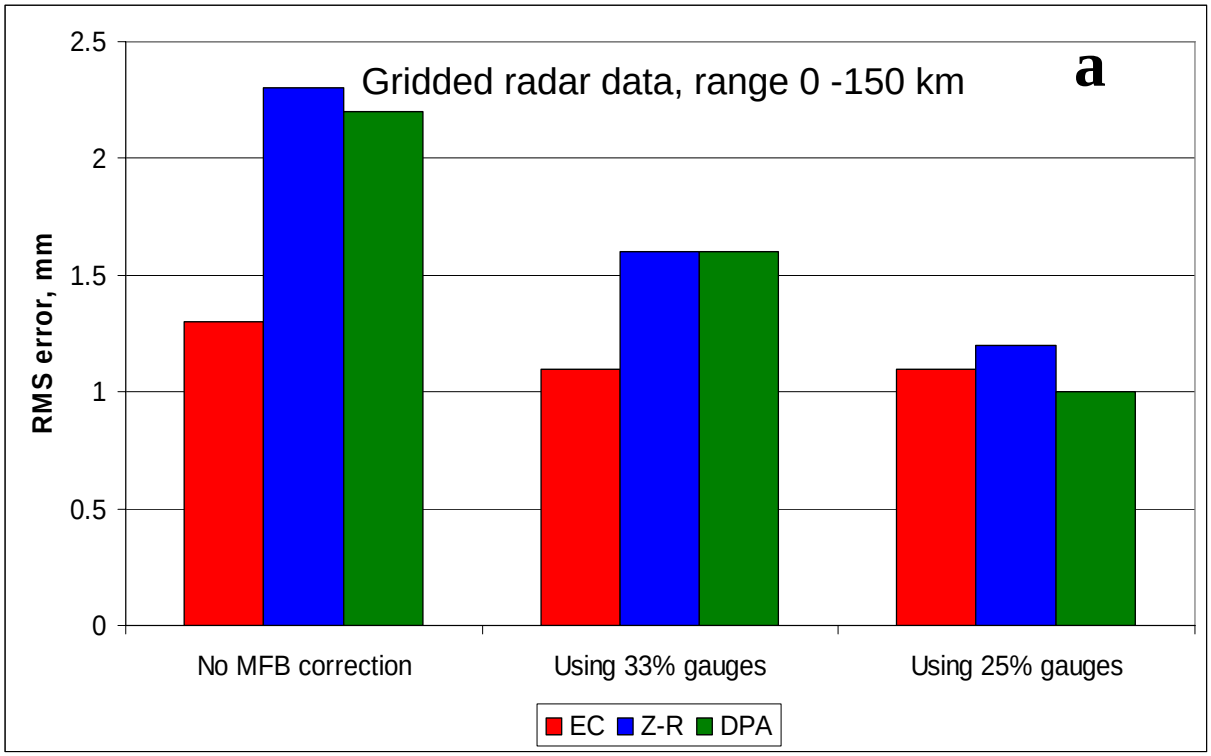

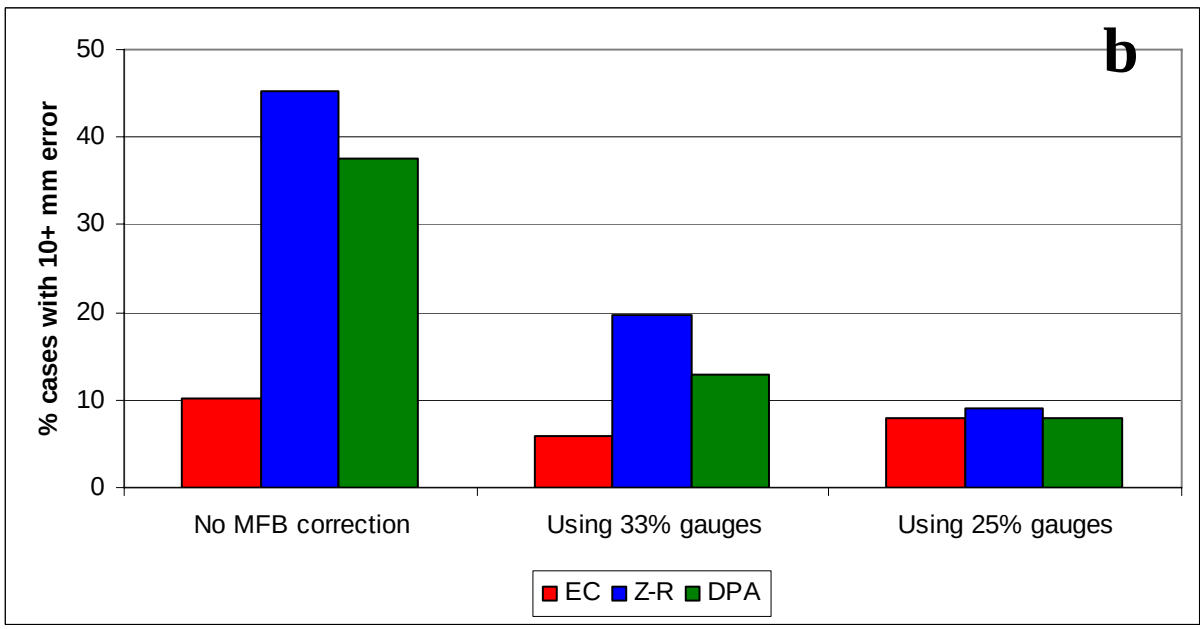

Figure 1-5. As in Fig. 1-3, except data are the gridded dataset 2003-2005. RMS errors (a) are from 4675 cases < 150 km from the KTLX WSR-88D unit; percent cases with 10-mm errors (b) are from 117 cases with precipitation estimates > 10 mm.

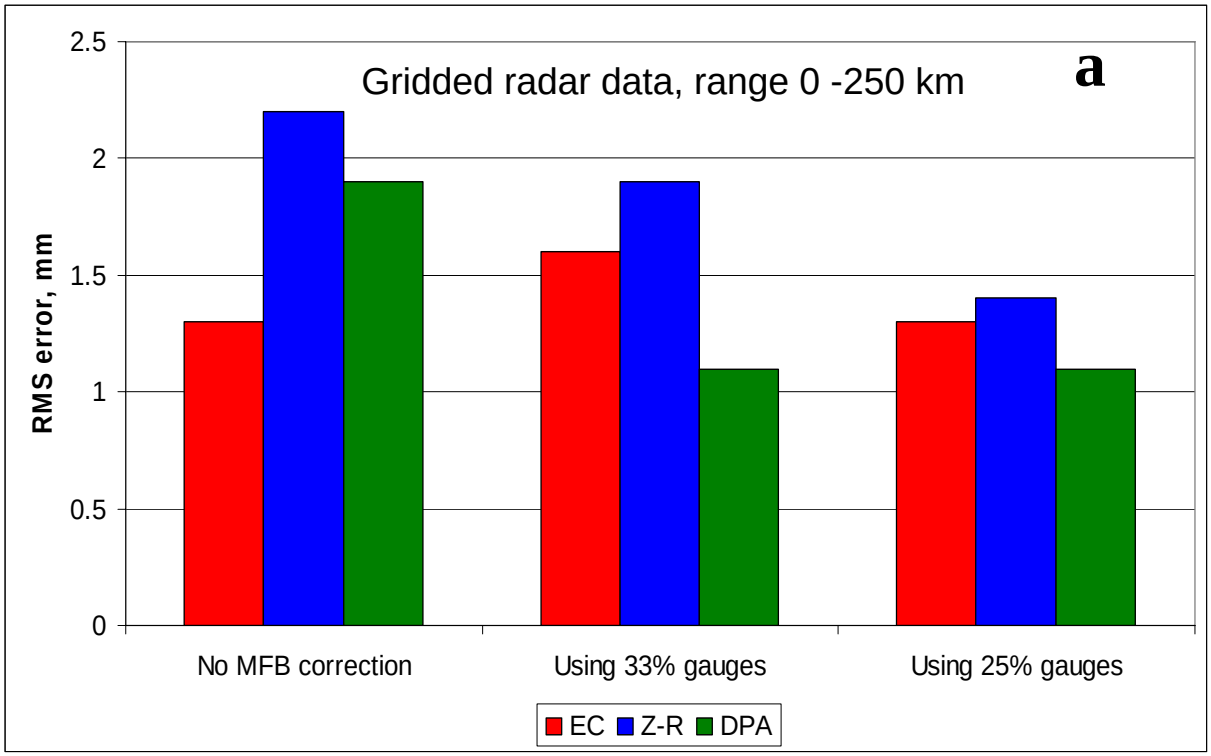

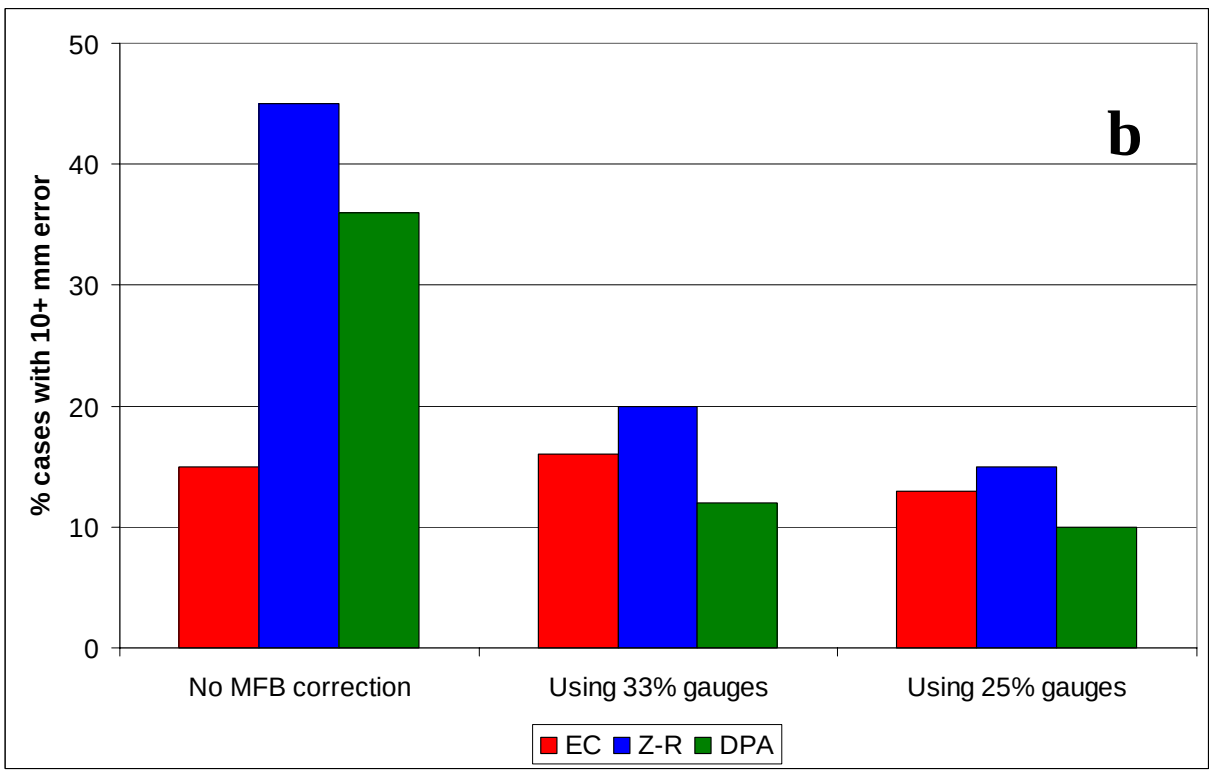

Figure 1-6. As in Fig. 1-4, except data are from selected events 2003-2005. RMS errors (a) are from 8451 cases < 250 km from the KTLX WSR-88D unit; percent cases with 10-mm errors (b) are from 171 cases with precipitation estimates > 10 mm.

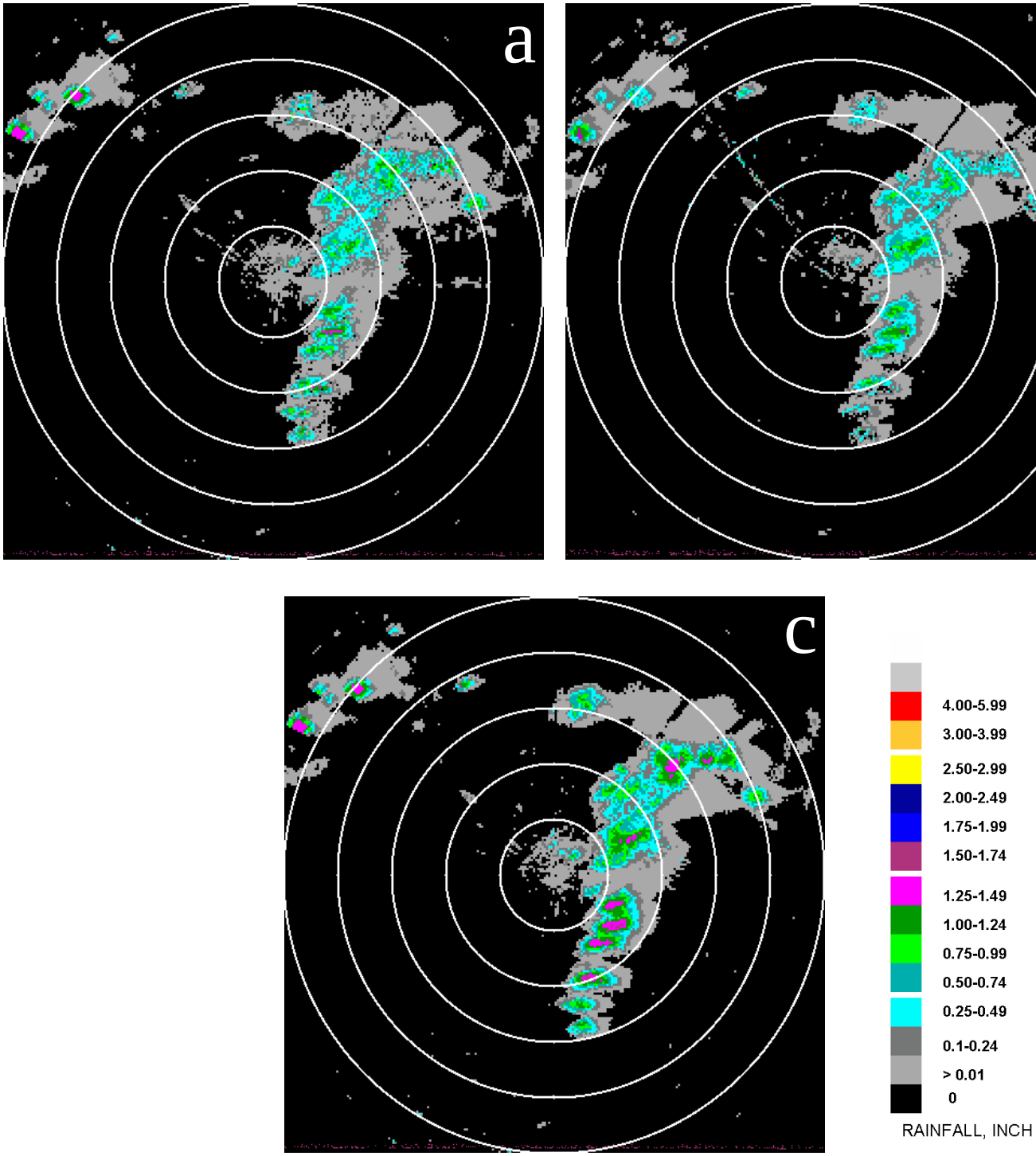

Figure 1-7. One-hour precipitation within the KOUN umbrella, valid 0000 UTC 22 April 2004. Images are from (a) dual-polarization "Combined" algorithm QPE1, (b) newer algorithm EC and (c) Z-R horizontal polarization relationship. Range rings are at 50-km intervals.

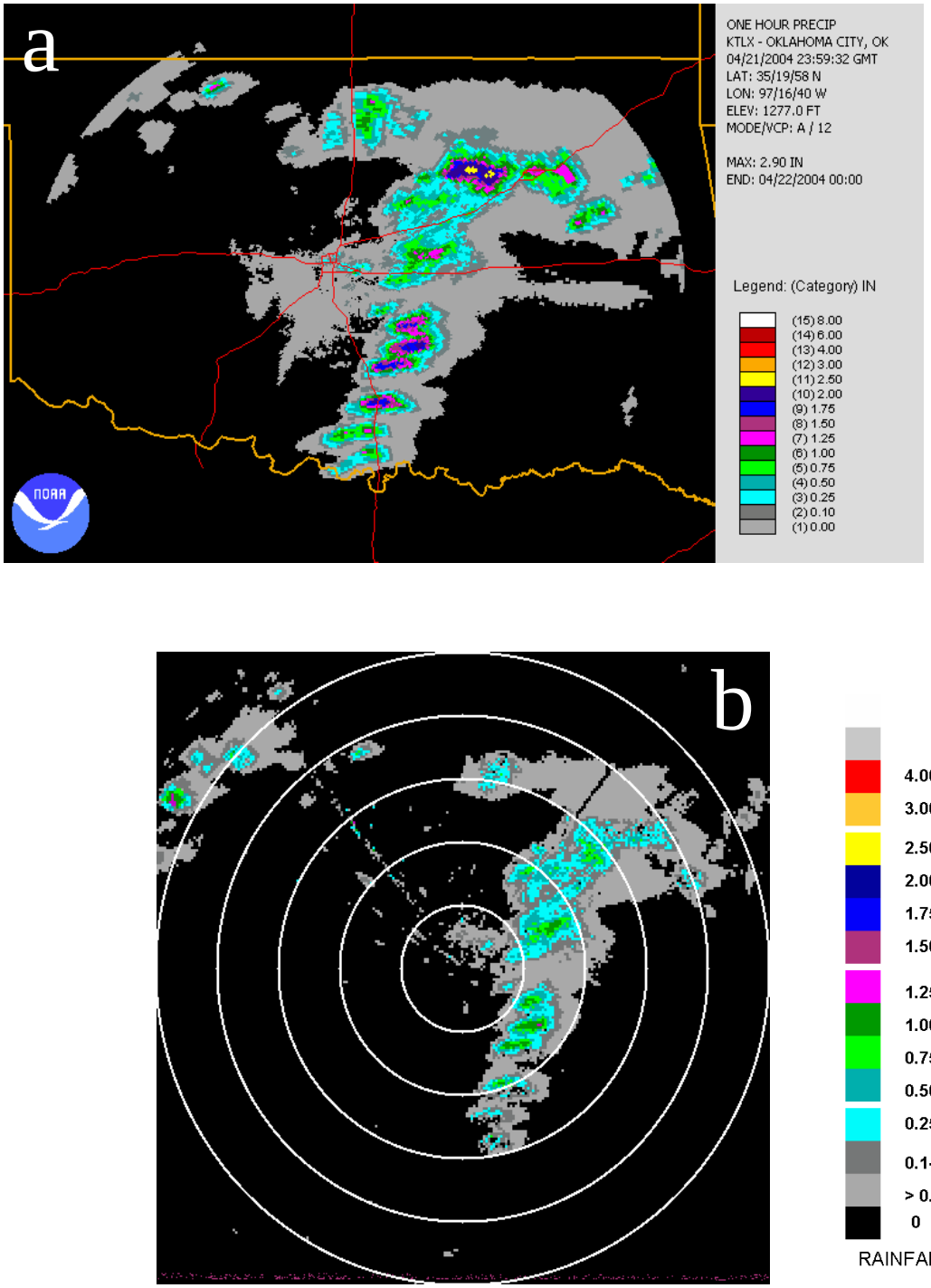

Figure 1-8. (a) One-hour precipitation (OHP) from the operational KTLX WSR-88D, valid 0000 UTC 22 April 2004 (b) One-hour precipitation within the KOUN umbrella, newest algorithm EC version.

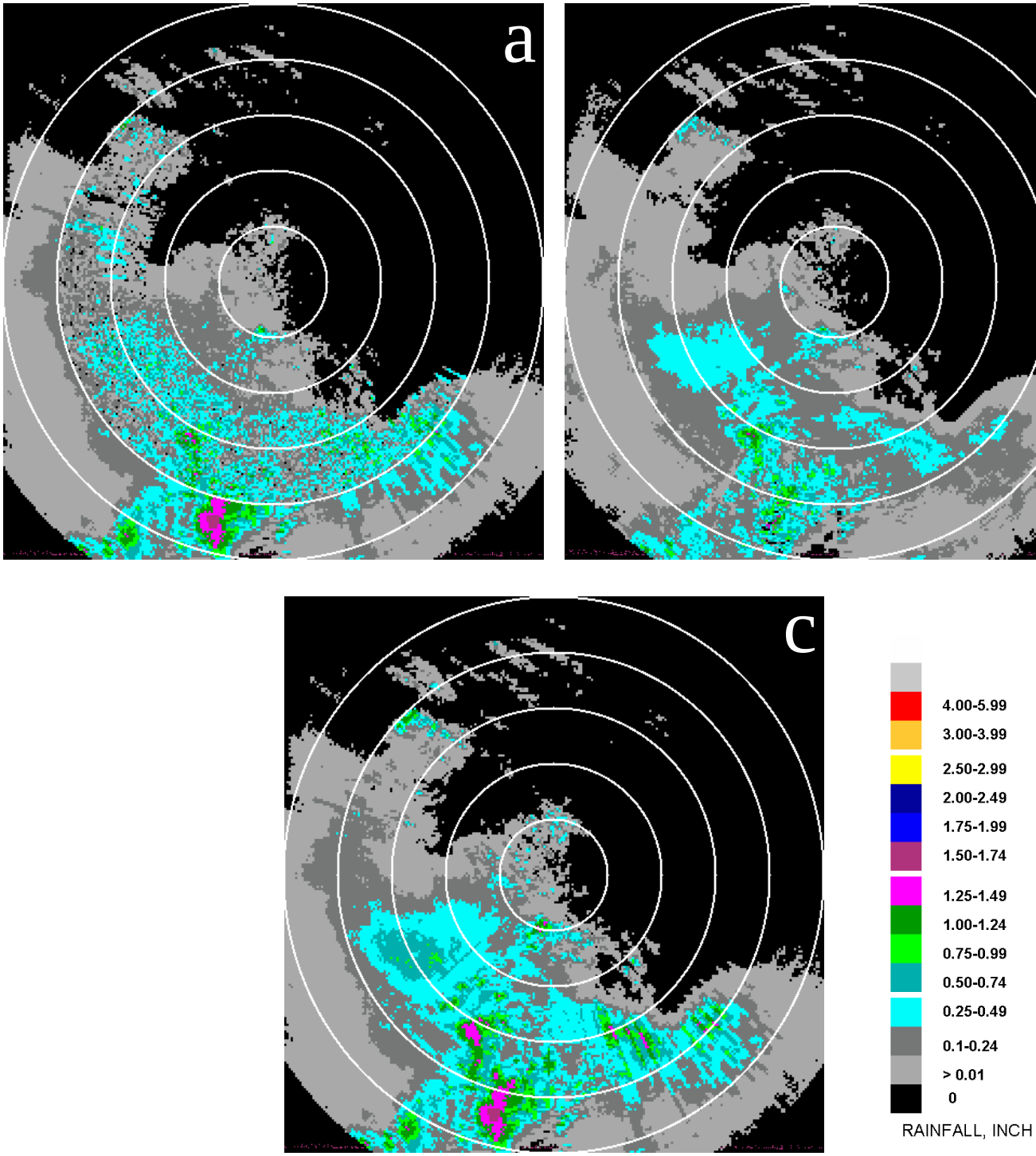

Figure 1-9. As in Fig. 1-7 except for 0300 UTC, 3 June 2004.

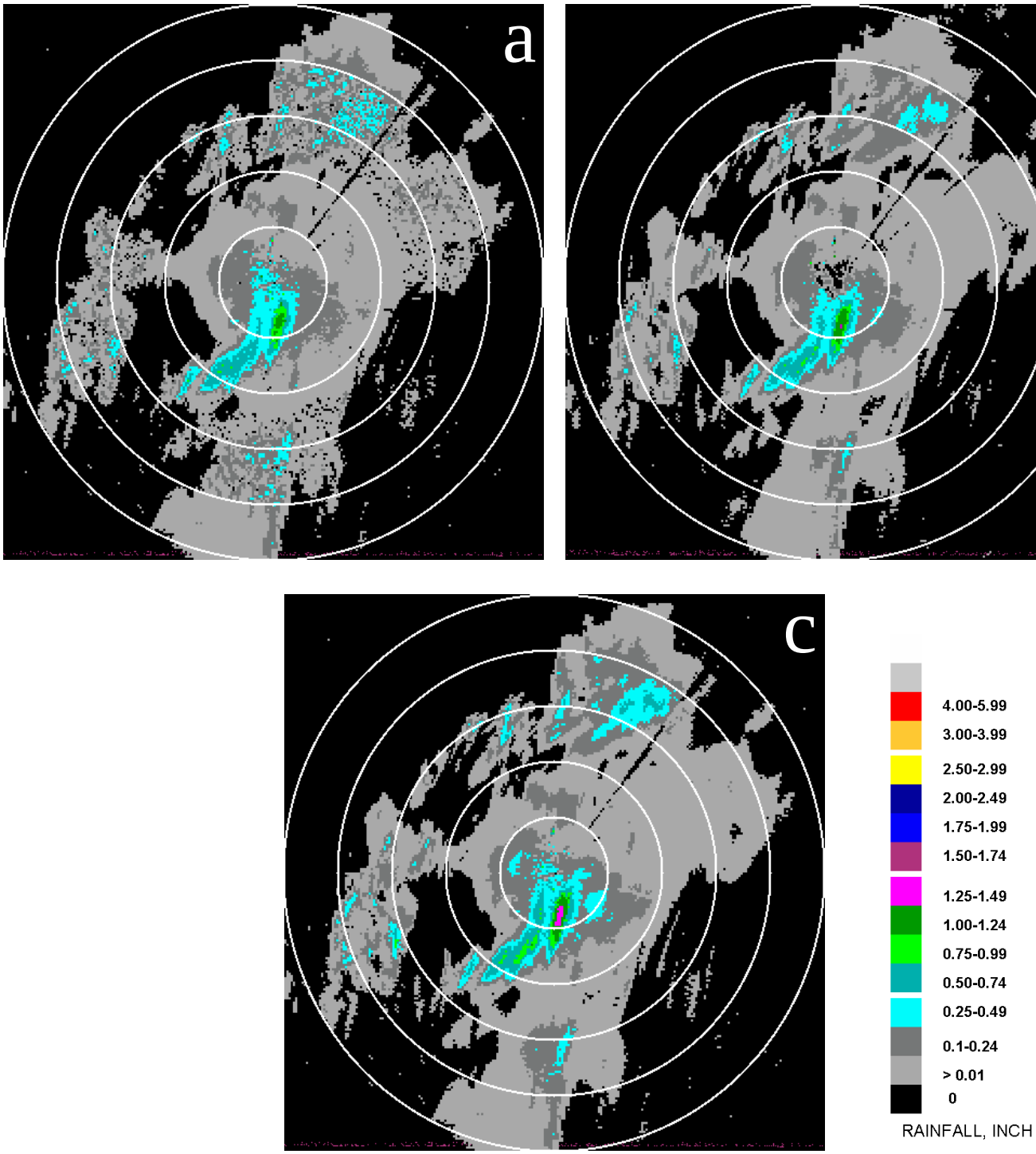

Figure 1-10. As in Fig. 1-7 except for 1600 UTC, 9 June 2004.

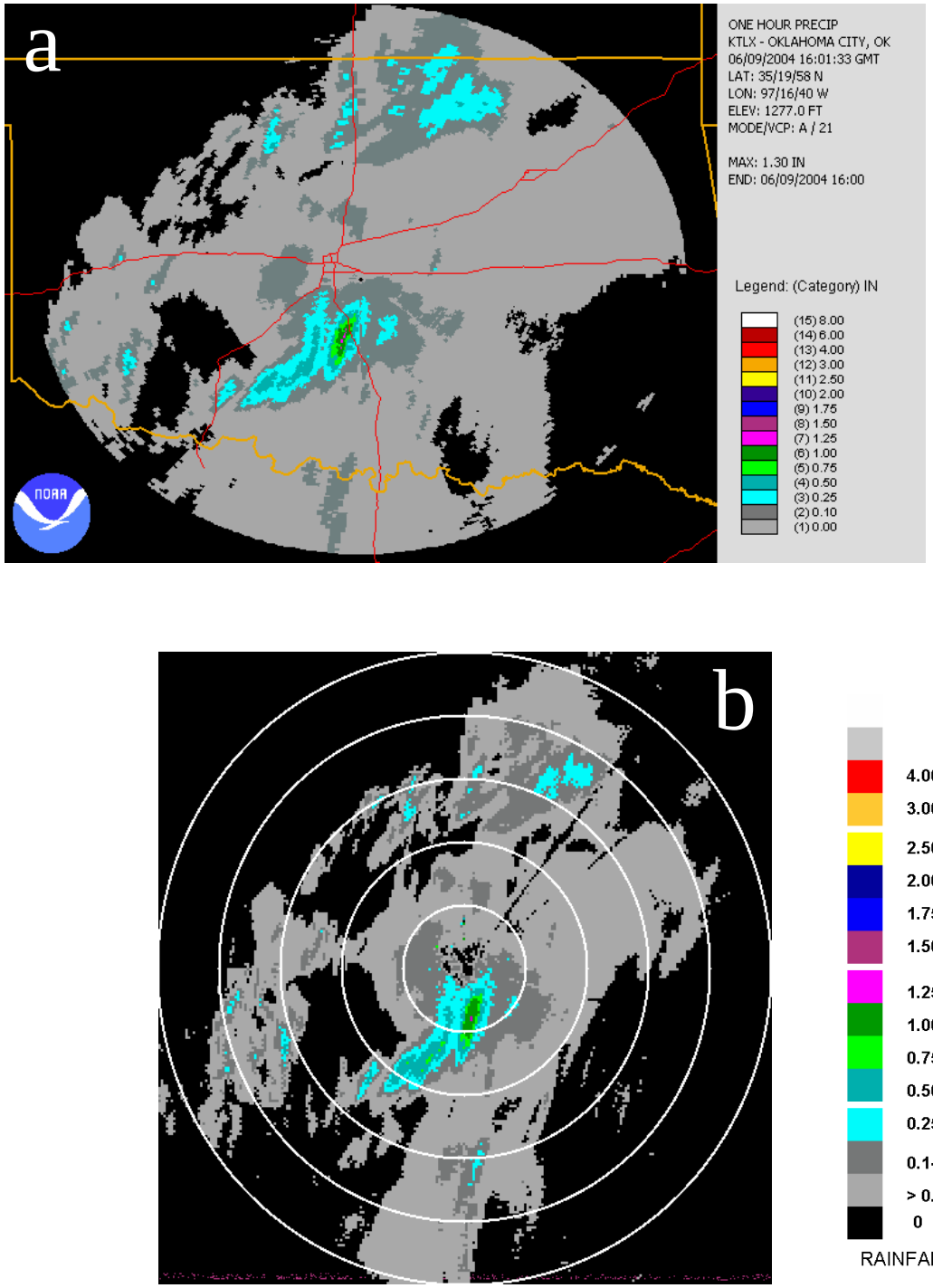

Figure 1-11. As in Fig. 1-8 except for 1600 UTC, 9 June 2004.

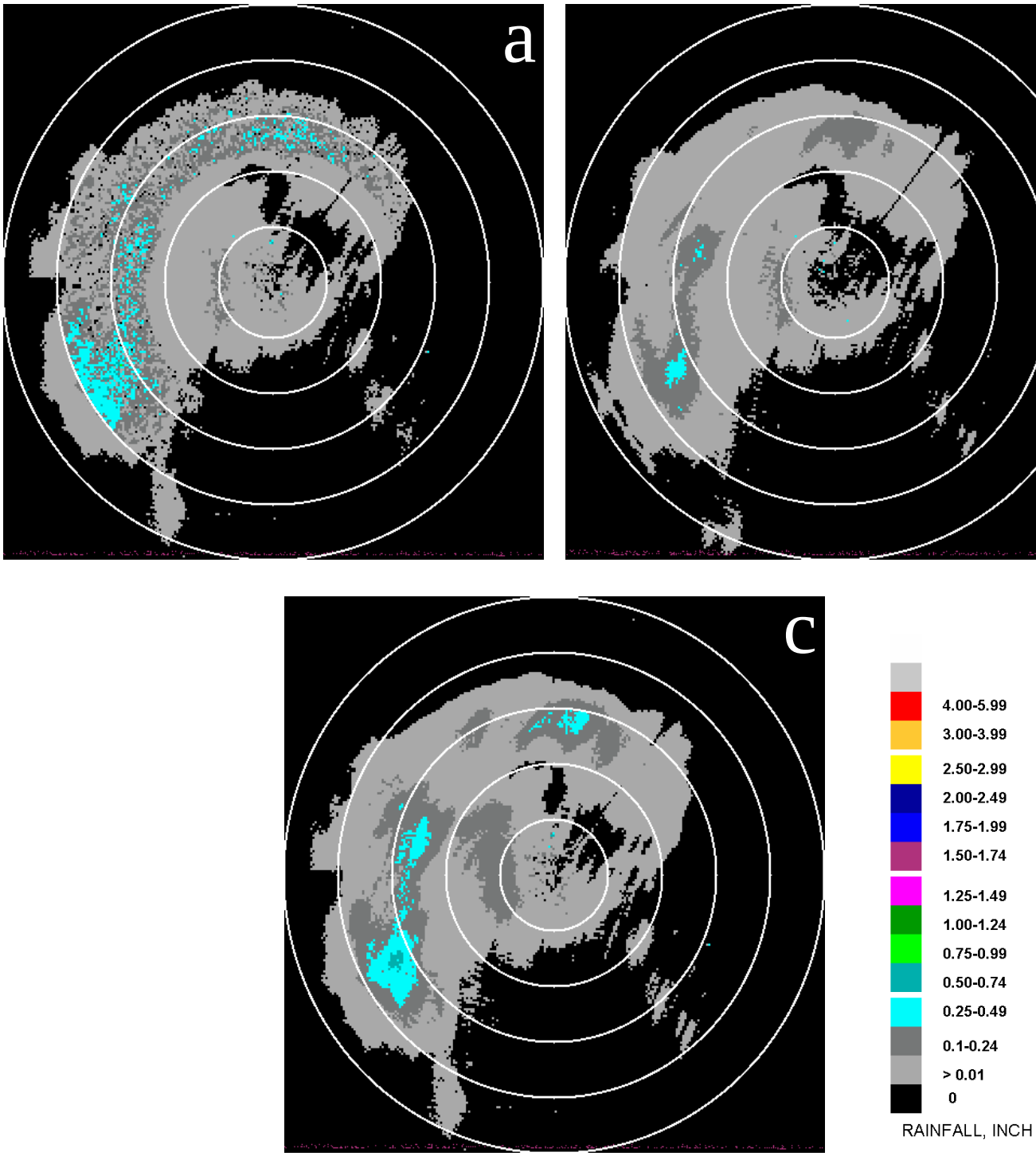

Figure 1-12. As in Fig. 1-7 except for 1200 UTC, 15 November 2004.

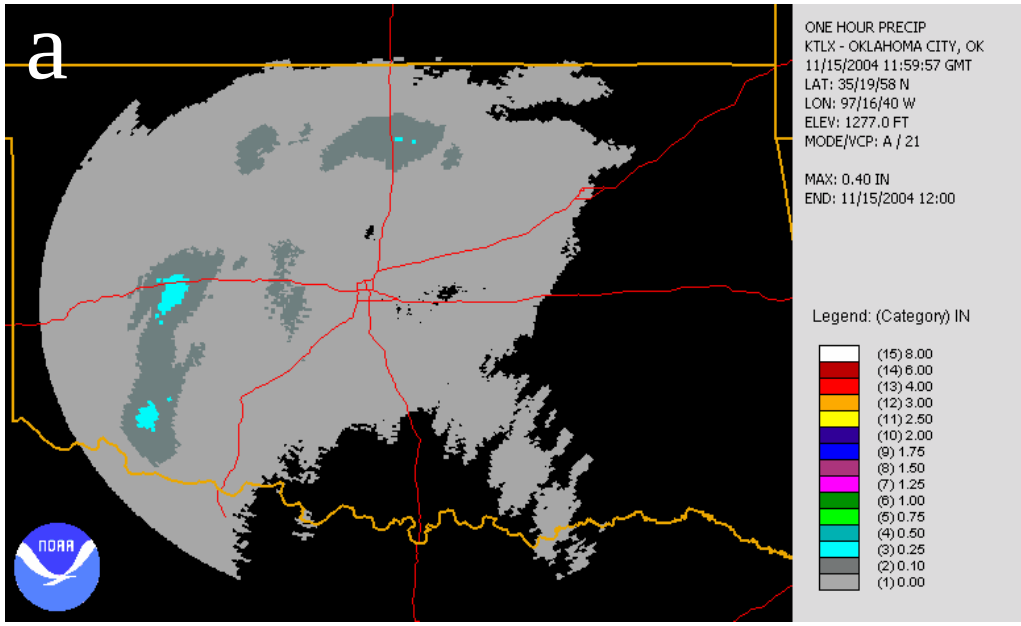

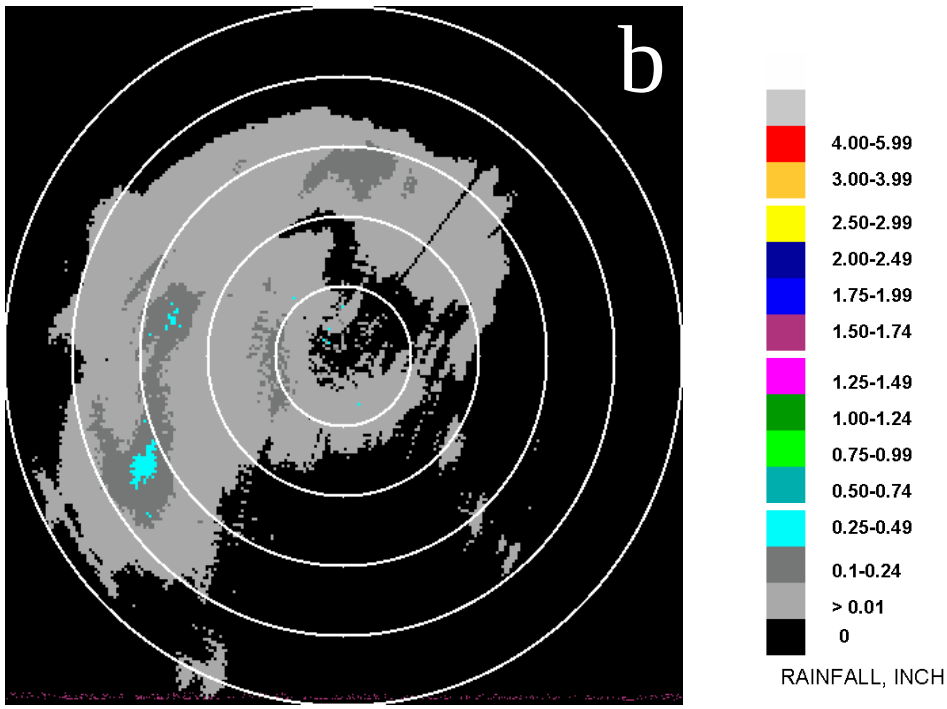

Figure 1-13. As in Fig. 1-8 except for 1200 UTC, 15 November 2004.

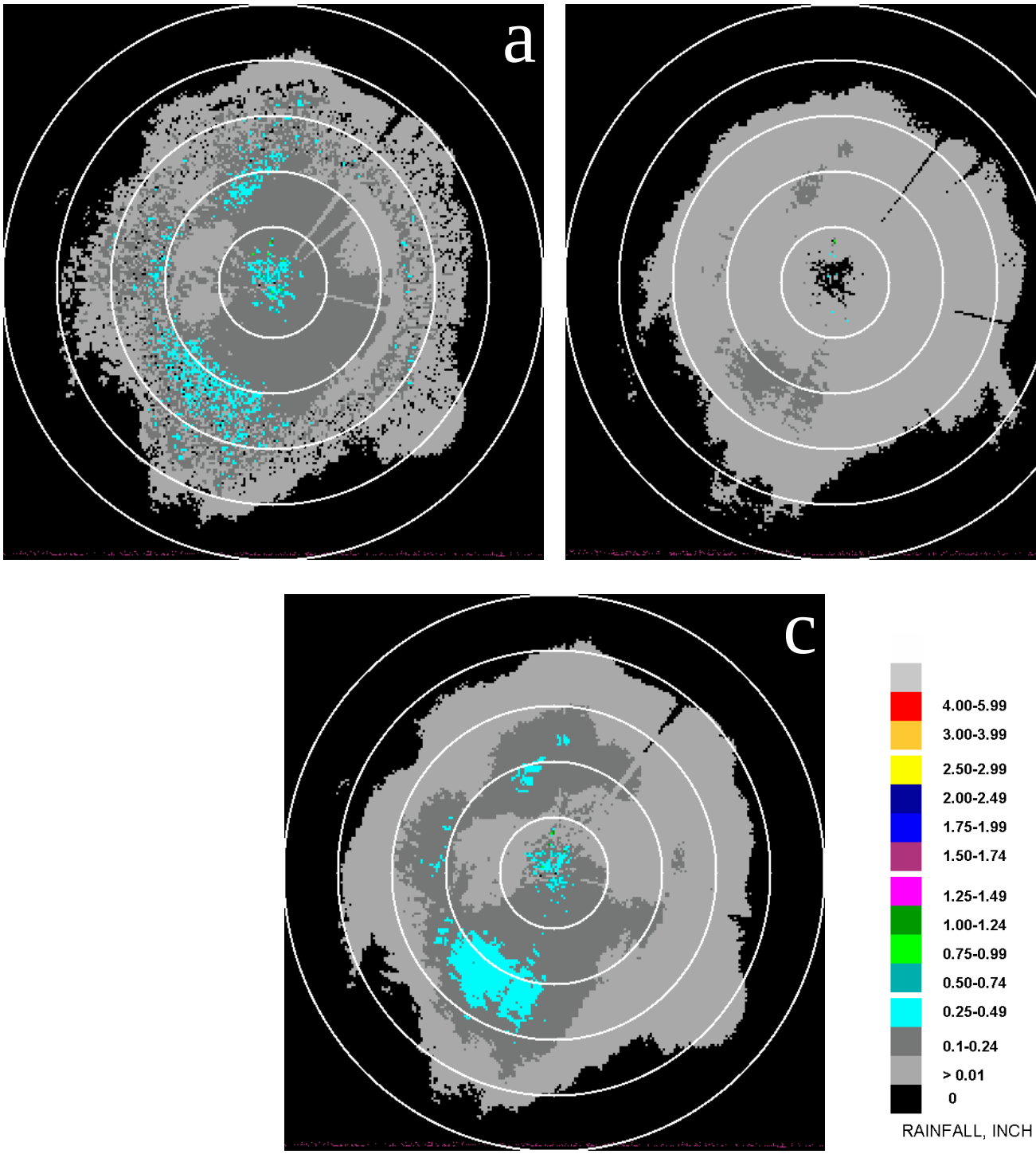

Figure 1-14. As in Fig. 1-7 except for 0900 UTC, 6 February 2005.

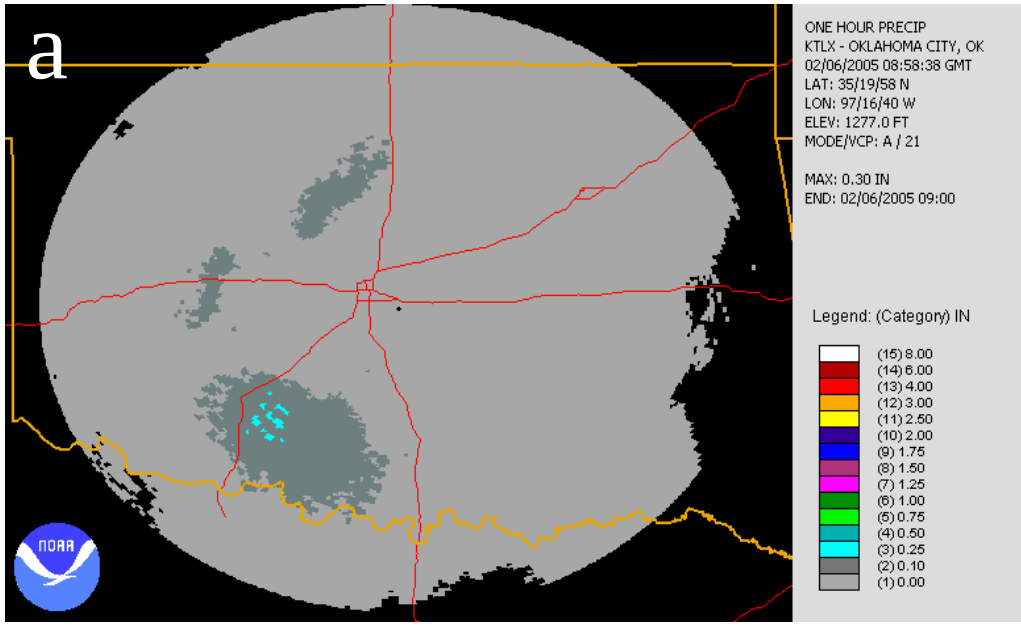

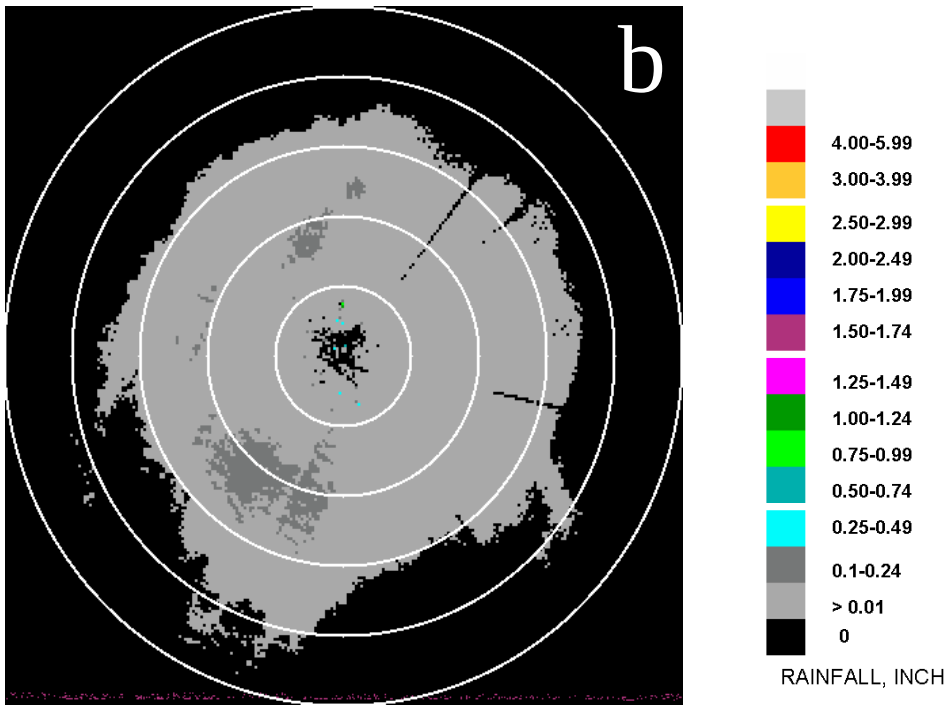

Figure 1-15. As in Fig. 1-8 except for 0900 UTC, 6 February 2005.

Task 1.1 Part II: Application of EC (Echo Classification) Rainfall Algorithm To NCAR S-pol Data from Florida During 1998

Introduction

Prior to the introduction of the proposed EC (or Echo Classification) algorithm in February 2007, our effort at validation of the QPEv1 algorithm using Florida NCAR S-Pol data was concentrated on the difficult problem of deriving rainfall estimates from the specific differential phase (Kdp) moment. As noted by NSSL developers regarding the Oklahoma data, this moment might yield more reliable estimates in hail areas, but elsewhere tends to produce noisy precipitation fields.

With the incorporation of the latest, EC version for dual-polar precipitation estimation in our study, consideration must be given to the fact that the algorithm normally depends on the Hydrometeor Classification Algorithm (HCA), to account for the wide range of possible hydrometeor and other target types. In the situation of warm season rainfall in the central Florida peninsula, however, melting/freezing processes play very little role, as hail is relatively rare and the melting layer is high. Hence, if biological targets and AP/clutter are ignored, we believe we can approximate the EC algorithm to the sub-component based upon reflectivity/differential reflectivity, or R(Z,Zdr), which should cover the majority of environmental circumstances encountered. Hence, that sub-component will be used exclusively here, in lieu of the complete HCA/EC evaluation. The dual-pol data used in this portion of our study were collected from the NCAR S-Pol radar situated about 26 km SSW of the operational WSR-88D station in Melbourne, FL (KMLB) during the period July 28 – Sept 26, 1998. Hereafter, the two datasets are referred to as SPOL and KMLB, respectively. The results to be presented are from a set of 60 hours from 21 study days.

Operational characteristics of the S-Pol unit during this period can be found at http://www.eol.ucar.edu/rsf/spol/spol.html. A description of parallel results obtained on two study days appears in Dixon et al. (2007).

Our goals in this phase of the dual-polarization study include confirmation that the EC algorithm yields realistic and reliable results in an environment outside Oklahoma, that the relationship between dual-polarization and horizontal polarization estimates is similar in Florida and Oklahoma, and to determine if the absolute accuracy of the estimates is improved by the introduction of dual-polarization information.

2.1 Overview of Findings

Initial indications are that, while the EC logic was developed and optimized for the NSSL KOUN dual-pol radar in the predominantly convective environment of the central U. S. Great Plains, the application of the analogous logic of the R(Z,Zdr) algorithm to the NCAR S-Pol, dual-pol dataset yields consistent and comparable results in the tropical environment of central Florida. In both systems/locations, the statistical relationship of dual pol-derived precip to traditionally derived (i.e. Z-R) estimates is comparable;

likewise for the relationship of dual pol-derived hourly precipitation estimates to hourly, co-located rain gage reports. And in individual case studies, rainfall amounts and patterns revealed in images from the dual-pol experimental radar against analogous images from the nearby WSR-88D operational system (SPOL vs. KMLB); KOUN vs. KTLX (Oklahoma City, OK), are, overall, similar.

Some regional differences were observed. While both the dual-pol radars in Oklahoma and Florida give lower, overall estimates of precipitation than their counterpart WSR-88D systems, the Florida (S-Pol) system underestimates to a greater degree, particularly with regard to the EC (or analogous R(Z, Zdr)) field. Paradoxically, radar-based rainfall accumulation images from the dual-pol radars generally reveal greater areal precipitation coverage (though in the very light ranges) than do their counterpart images from the WSR-88D radars. These issues will be discussed below.

2.2 Dual-Pol vs. Single Pol Behavior in Florida (SPOL) and comparison to Oklahoma (KOUN)

Fig. 2-1a shows the relationship between dual-polarized (i.e. EC) and horizontally-polarized (i.e. R(Z)) hourly precip estimates from the experimental radar KOUN in Norman, OK, while Fig. 2-1b shows the same relationship (with R[Z;Zdr] substituting for the EC as discussed above) from the experimental SPOL radar in Melbourne, FL, for all estimates throughout the July 28 – Sept 26, 1998 period. The two scatter diagrams are very similar in that they both consistently show lower estimates for the dual-pol based rainfall than that from the traditional, R(Z) relationship, though a little less so for the SPOL radar. Here, Multiplicative Bias (MB)=0.89; Arithmetic Bias (additive bias, B)= -0.38. These were lower than for the KOUN radar (MB=0.72; B= -1.25). Note that a negative value of Arithmetic Bias here indicates dual-pol estimates are less than single pol, on average. There are some differences, however: the KOUN radar shows wider scatter, in general, and more datapoints where the dual-pol estimate exceeds the single-pol estimate in the lower precip ranges (up to about 6 mm), while the SPOL radar shows more points where the dual-pol estimate exceeds the single-pol estimate in the higher precip ranges (above 6 mm).

Fig. 2-2 is analogous to Fig. 2-1b for the SPOL radar in Florida, although it now compares the dual-pol (R(Z;Zdr))-based estimates to the those from the Hourly Digital Precipitation Data Array (DPA) product of the nearby KMLB, after the SPOL estimates have been translated to the same, 4-km HRAP grid as the DPA. Here, we see a somewhat greater, negative departure of the dual-pol based rainfall (MB=0.75; B= -1.08) than when compared to the single-pol estimates from the same radar (i.e. MB=0.89; B= -.39). Indeed, the greater portion of the relative underestimation of the SPOL R(Z;Zdr) vs. the KMLB DPA is attributable to inherent differences between the SPOL and KMLB radars, as opposed to differences resulting from the use of a dual-pol R(Z;Zdr) vs. single (horizontal) pol estimation. These inherent differences may have several explanations, one of which may be that the SPOL radar registered lower than KMLB during all or part of the period July 28 – September 26, 1998. In a calibration check conducted on the S-Pol radar during the July-September 1998 experiment, it was estimated that the radar

reflectivity was, on average, 0.65 dB too low (range: 0.45-0.85 dB). This average calibration difference was added back to the reflectivity measures before processing in NCAR's experiments (Brandes et al. 2002).

2.3 Individual Florida Cases: Examination of Radar (SPOL) vs. Radar (KMLB) Scatter Diagrams

Next, SPOL-based estimates are compared to KMLB-based DPA estimates (as in Fig. 2-2), but for six, individual cases. Note that the six cases, or individual hours, were chosen because they had widespread or substantial precipitation or were indicative of a situation that persisted for several hours, but with no a priori knowledge of the relative QPEs of the SPOL vs. KMLB radars.

Fig. 2-3a shows the distribution of DPA for the hour ending 8/20/98 19:00 UTC against the analogous, SPOL-based R(Z), while Fig. 2-3b shows the DPA against the SPOL-based R(Z; Zdr). Note that in this instance, the agreement between DPA and SPOL is very close, with SPOL R(Z) just slightly exceeding DPA (MB=1.02; B= +.07) and SPOL R(Z;Zdr) just slightly under it (MB=.95; B= -.18).

In Figs. 2-4a-b, we see the same comparisons for the hour ending 9/05/98 20:00 UTC with almost an identical outcome, i.e. with SPOL R(Z) just slightly exceeding DPA (MB=1.06; B= +.22) and SPOL R(Z;Zdr) just slightly under it (MB=.93; B= -.26). Then in Figs. 2-5a & b, we see the comparisons for the hour ending 9/19/98 19:00 UTC, with the opposite result now seen as in the bulk analysis of Fig 2-2 – i.e. the SPOL estimates exceeding – indeed, well exceeding - the DPA for both R(Z) (MB=1.41; B= +.99) and R(Z;Zdr) (MB=1.34; B= +.81). And in Figs. 2-6a-b for the hour ending 9/20/98 19:00 UTC (i.e. exactly one day later), we still see the SPOL estimates exceeding the DPA for both R(Z) (MB=1.09; B= +.33) and R(Z;Zdr) (MB=1.01; B= +.05), though not by as much.

Of these six cases, in only two did the results turn out in the same sense as they did in the bulk analysis of the Melbourne cases – i.e. with the SPOL-based R(Z;Zdr) estimate being significantly less than the DPA. In Figs. 2-7a-b for the hour ending 7/28/98 23:00 UTC (note: a case with not very widespread precip), we have (MB=.84; B= -.53) for R(Z) and (MB=.65; B= -1.14) for R(Z;Zdr), while in Figs. 2-8a-b for the hour ending 9/25/98 23:00 UTC, we have very sharp underestimations of (MB=.58; B= -2.18) for R(Z) and (MB=.54; B= -.2.35) for R(Z;Zdr).

So, overall, the six individual cases show a fairly wide range of behavior, with the SPOL-based estimates (both R(Z) and R(Z;Zdr) exceeding the DPA in one instance (i.e. 9/19/98 19:00 UTC (Figs. 2-5)); with the opposite being true in two instances (i.e. 7/28/98 23:00 UTC (Fig. 2-7) and, particularly, 9/25/98 23:00 UTC (Fig. 2-8)); and with both sets being fairly equivalent in the other three cases. In all instances except the two extreme cases, the SPOL estimates exceed the DPA at low precip rates but are less than the DPA at the higher rates (and with SPOL R(Z;Zdr) always being less than the SPOL R(Z)). Thus, what we may be seeing here is that the SPOL estimates - particularly the R(Z;Zdr) - are yielding a somewhat different distribution of rainfall across the intensity spectrum, which

may or may not be more realistic than the estimates provided by the operational WSR-88D.

Another finding that needs to be addressed is the rather wide departure of the two "extreme" cases, with R(Z;Zdr) well exceeding DPA across the intensity spectrum for 9/19/98 19:00 UTC, but the opposite being observed for 9/25/98 23:00 UTC. This brings a couple of possible explanations to mind: one is that the meteorological/environmental conditions were different on these two days, in such a way that the differences between the two radars/algorithms were accentuated (in opposite directions on the two occasions); another possibility is that the two radars were calibrated differently on these days, with the experimental SPOL radar being the one more likely to be experiencing swings in its calibration. It is also possible that drop-size distributions never encountered in the KOUN development dataset appeared here.

When we revisit Fig. 2-2, we see that for all the SPOL R(Z;Zdr) vs. KMLB DPA hourly estimates considered "en mass", the SPOL estimates were lower, with an MB of 0.75 and an Arithmetic Bias of -1.08 mm. This may indicate that atmospheric/ hydrometeorological conditions which supported the KMLB radar yielding higher precip estimates than the SPOL predominated during the period of record (i.e. July 28 – September 26, 1998).

2.4 Examination of Radar (SPOL) vs. Radar (KMLB) Hourly Accumulation Images

To gain more insight, coincident hourly accumulation images from the two radars were next compared (after translation to the same, HRAP grid). Our aim was to confirm that the overall precipitation patterns were similar, and to identify any persistent patterns of differences between the two radars.

In Fig. 2-9a-d, we see the estimates for a) KMLB DPA; b) SPOL R(Z); c) SPOL R(Z;Zdr); and d) Comparison of a and c, respectively, for the case 8/20/98 19:00 UTC (i.e. corresponding to Figs. 2-3a&b). In the Comparison image (Fig. 2-9d), areas where both radars perceived measurable precipitation are shown in blue; areas where only SPOL R(Z;Zdr) perceived it are shown in violet, and areas where only KMLB DPA perceived it are shown in green. The first thing to notice is that areas with measurable precipitation only in KMLB DPA occur exclusively at the outer ranges. This is, indeed, because the coverage range for precip analysis of the operational KMLB is greater than that for the SPOL (i.e. 230 km vs. 171 km). On the other hand, within the 171 km range ring, areas where both radars or only SPOL R(Z;Zdr) reveal measurable precipitation are predominant, whereas areas where only KMLB DPA reveal it are very rare. The reason for this apparent discrepancy within the (171 km) range of mutual coverage – except right near the respective radars - is primarily a consequence of a disparity in the manner by which the two sets of images are processed, whereby the cutoff for the lowest "displayable" (i.e. non-background black) value of the DPA products is higher than that for the SPOL (i.e. ~.3 mm vs. .1 mm). Another way of perceiving this is that the SPOL images reveal "trace" accumulation amounts whereas the DPAs do not. So unfortunately,

not much can be surmised from these difference fields. It should be noted that above this lowest precip level, the quantizations of the remaining levels (i.e., colors) are the same.

In comparing the remaining sets of images for the 8/20/98 19:00 UTC case, it is seen that Figs. 2-9a & b (i.e. KMLB DPA vs. SPOL R(Z), with both being derived from the R(Z) relationship) yield comparable patterns and amounts except near the respective radars, where the SPOL image reveals echoes – often spiky – while the DPA image does not. This is, in part, because our processing of the SPOL accumulations does not have the benefit of the many quality control procedures contained in the operational, WSR-88D algorithm, and hence, AP and ground clutter are much more likely to be retained. Meanwhile, Figs. 2-9b & c (i.e. SPOL R(Z) vs. SPOL R(Z;Zdr)) yield a very close match in coverage and amount – which is to be expected since both are from the same radar and the latter is a function of the former – except with regard to the heaviest cores (i.e. > .50", appearing as oranges and reds), which are reduced in Fig. 2-9c at middle and outer coverage ranges compared to Fig. 2-9b**,** but are enhanced near the radar. The diminishing of the peaks at middle and outer ranges is a well known consequence – and likely, benefit – of the application of the R(Z;Zdr) dual-polar formulation vs. the single-polar R(Z). (No attempt will be made to explain the relative enhancement at close ranges this time.)

Analogous comparisons of the four panels for the other cases yield very similar results to the above, and so are not all shown. But it may be instructive to look at them for the two "extreme" cases., so as to perhaps gain additional insight.

Figs. 2-10a-d show the 4-image comparison for the case in which the SPOL estimates most exceeded the DPA (i.e. the hour ending 9/19/98 19:00 UTC, corresponding to Fig. 2-5, above). What stands out here is the very strong echoes right near the SPOL radar (and just SSW of the KMLB radar) which are considerably stronger in both the SPOL images (Figs. 2-10 b,c) – particularly R(Z;Zdr) – than they are in the KMLB DPA image (Fig. 2-10a). The most likely explanation is that heavy rainfall, as well as ground clutter, indeed existed in the immediate vicinity of the two radars and – for the reasons mentioned above (i.e. better quality control and more filtering near the operational WSR-88D) – the SPOL radar accentuated these echoes considerably more so than did the KMLB. And since accumulations are comparatively modest in the remainder of the mutual coverage area of the two radars, these stronger echoes near the SPOL radar predominate the statistics, resulting a mean-field bias exceeding one and a positive value of arithmetic bias (i.e. MB=1.34; B= +.81 for the R(Z;Zdr) vs. DPA radar-radar comparison).

Figs. 2-11a-d show the 4-image comparison for the case in which the SPOL estimates were the most below the DPA (i.e. the hour ending 9/25/98 23:00 UTC, corresponding to Fig. 2-8, above). Here, what stands out are two W-E aligned bands, one northwest to northeast of the radars and another south of them, which are much stronger in the DPA image than in either of the SPOL images. Since these bands are not too close to the radars, speculation here is that the DPA product from the WSR-88D radar, which scans up to 3.5 degrees elevation in its precip processing, is picking up strong echoes aloft – perhaps due to hail – that are not observed by the SPOL radar, which only processes

rainfall at 0.5 degrees elevation in the analysis system used for this study. (Thus this may, indeed, be a situation where our analysis of the SPOL precipitation – both R(Z) and R(Z;Zdr) – was hindered by our assumption that hail is rare in late summer, tropical Florida, and that we could forego preceding our QPE analysis with an HCA determination.)

In summary of the (6) individual cases, the hourly accumulations from the two radars (KMLB and SPOL) are generally quite similar in pattern, and usually in amount, as well. Differences are more discernible between the single-pol KMLB images and (both) the SPOL images than they are between the single- and dual-pol SPOL images, themselves. This is because: a) the DPA images from KMLB cut off "trace" levels of accumulation from the display; while the SPOL images do not; b) The WSR-88D algorithm has quality control steps which filter AP and clutter – particularly near the radar, while our processing method used for the SPOL accumulations does not; and c) The WSR-88D algorithm processes its precipitation based upon a "Hybrid Scan" composite of the lowest four elevations (i.e. 0.5 to 3.5 degrees) while the SPOL algorithm is based only upon the 0.5 degree elevation scan. In the cases where the accumulation from one system is significantly different than the other, statistically, it appears that a small area or areas of heavy echoes predominated, and that these echoes were far more enhanced in one system than the other, for the reasons stated above.

2.5 Comparison between Radar and Rain Gage Observations

In order to determine which estimates may have been closer to "ground truth", the results from all the precip events in the vicinity of Melbourne, FL during the study period of July 28 – Sept 26, 1998 were next compared to hourly rain gage reports. Gages that were employed in the Tropical Rainfall Measuring Mission (TRMM) for use in Ground Validation of experimental satellite precip estimates (i.e. TRMM-GV gages) were obtained from the website http://trmm-fc.gsfc.nasa.gov/trmm_gv/index.html and collocated with the radar estimates. A total of 1566 "gage-radar pairs", for which both the gage report and the nearest HRAP gridpoint estimate had non-zero precip, were found during the above period. (See Fig 2-12 for the locations of these gages.)

In Fig. 2-13, we see scatter diagrams of one-hour precip estimates from (a) KMLB DPA (based on R(Z)); and (b) SPOL dual pol estimates (R(Z,Zdr)), each compared to the TRMM-GV one-hour gage report set. It is seen that in both instances, the radar precip estimates, in sum, were less than the gage reports, with MB substantially less than 1.00 and Arithmetic Biases (B) negative. Of these estimates, though, the KMLB DPA were closer to the gage reports (i.e. MB=.74; B= -1.31), than the SPOL dual pol (i.e. MB=.61; B= -1.95)

It is obvious that differing biases between the two radars have some effect on the overall interpretation. For most hydrologic applications, however, it is possible to estimate and then partially correct these biases by applying a multiplicative correction factor based on a set of recent gage-radar pairs. To facilitate our analysis, we therefore estimated a mean-field bias (MFB) correction for each hour's data for both radars, in a manner

analogous to that described in Section 1. The MFB was calculated as the mean gage amount divided by the mean radar amount at some gage locations where both radar and gage were nonzero; to approximate operational conditions where some gage reports are time-delayed, we employed only half the available gage sites, chosen at random.

The results of this correction are shown in Fig. 2-14 (which is analogous to Fig. 2-13). It is now seen that, while all the radar sets are still underestimating precipitation, in the mean, compared to the gages, they are now considerably closer, with statistics for KMLB DPA of (MB=.92; B= -.41) and for SPOL dual pol of (MB=.93; B= -.35). Note that the performance of the SPOL dual pol is now slightly better than that of the KMLB DPA (although single pol estimates provided by SPOL (not shown) now provide an even closer match to the TRMM gages, with (MB=.95; B= -.25)). An MB of unity is not achieved because not all gage/radar pairs were used in the MFB calculations.

A consideration of interest in hydrologic modeling is the degree to which the statistical distribution of the radar estimates approximates that of the coincident gage data, regardless of the correlation between the two sets of estimates. Since some hydrologic models are calibrated or designed based on gage observations, it is important that real-time input is statistically similar to that which would be supplied by gages. Therefore a percentile breakdown of all four of these datasets (i.e. the TRMM-GV gage and the three radar sets, above) was constructed, using the values obtained after MFB correction. In the traces shown in Fig. 2-15, it is apparent that the distribution of values in all four sets is fairly similar up to about the 80^{th} percentile. For the highest percentiles, the KMLB DPA estimates are closest to the gauge values, while the SPOL estimates are not as high as the gauge.

In this rather small sample of < 1600 gage/radar pairs, we cannot expect the gage and radar distributions to match at the very highest percentiles, where there are only a few cases. However, it is apparent that both the SPOL and KMLB estimates fairly well approximate the gage estimates up to about the 80^{th} percentile, and the KMLB estimates up to about the 90^{th} percentile. The SPOL output, for either single- or dual-polarization algorithms, appears to produce too few of the largest values, even after bias correction. It should be possible to adjust this feature through recalibration of the algorithm to better fit the regional rainfall climatology and radar unit calibration.

From this result, it becomes apparent that – at least in this study – the radar and its calibration, characteristics, etc., have a major impact in determining the precip estimate than does the fact of whether a single pol (R(Z)) or dual pol (R(Z,Zdr)) formulation is employed. It is also apparent that the biggest differences in the radar vs. rain gage estimates are provided by the heaviest rainfall samples.

2.6 Summary and Conclusions

In summary, we conclude that:

The EC algorithm will produce reliable, realistic results when ported to a subtropical regime;

The relationship between EC and standard convective Z-R estimates from the same radar unit is similar in Oklahoma and Florida, i.e., the dual-polarization algorithm tends to reduce the magnitude of the higher-rain rate Z-R estimates;

When comparing estimates from the neighboring KMLB and SPOL units, differences in amount and distribution of precipitation estimates in this study are largely attributable to inherent differences between the two radars and their operational characteristics, quality control procedures, etc.. These functional differences partially obscure differences between the EC algorithm and the Z-R algorithm;

The largest differences in the dual-pol radar vs. rain gage estimates appear in the heaviest rainfall events;

Recalibration of the multiplicative and exponential parameters in at least the R(Z,Zdr) component of EC, and possibly others, will be necessary to achieve maximum benefit from the dual-polarization upgrade in all locations.

Acknowledgements

We are indebted to Scott Ellis for his assistance in obtaining and interpreting the S-pol data, for providing background on the 1998 field experiments, and for reviewing this report.

References

Brandes, E.A., G. Zhang and J. Vivekanandan, 2002: Experiments in rainfall estimation with polarimetric radar in a subtropical environment. *J. Appl. Meteor*., **41**, 674-685.

Dixon, M., C. Kessinger, S. Ellis, G. Meymaris, J. Hubbert, and J. Van Andel, 2007: Improving NEXRAD data: Data quality algorithm progress (FY 2006 Annual Report). Report to NWS Radar Operations Center, 194 pp. [Available from http://www.eol.ucar.edu/rsf/NEXRAD/NexDQ_fy06/FY06_report7.pdf]

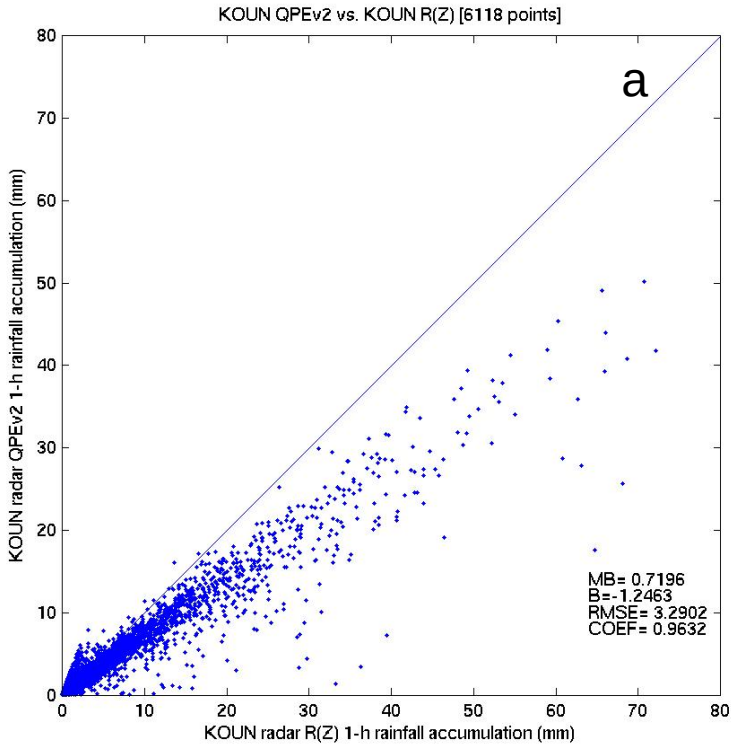

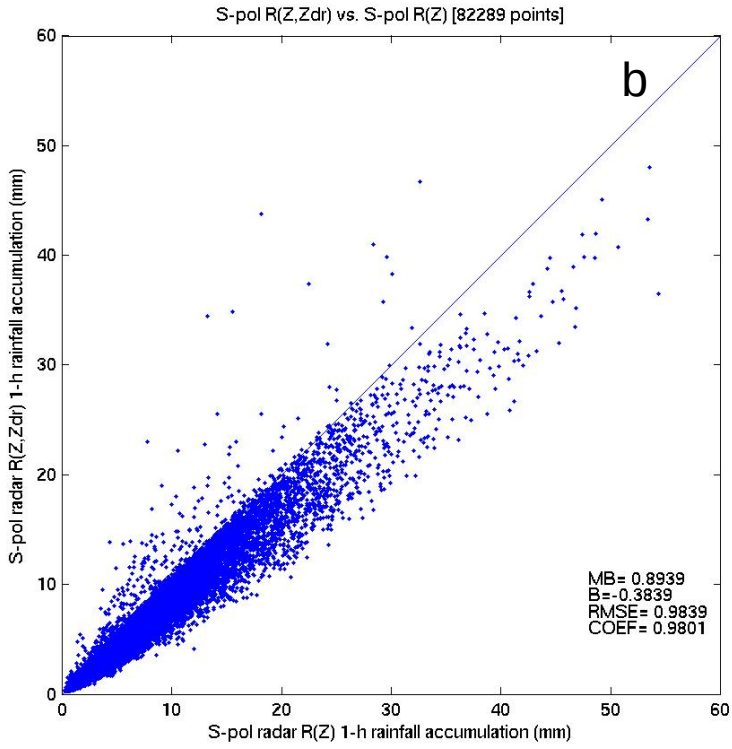

Fig. 2-1: Intra-radar (dual pol vs. horizontal pol) one-hour precipitation comparisons for each of experimental radars (a) KOUN, Norman, OK (i.e. EC (QPEv2) vs. R(Z) for 46 precip events during 2002-2005) and (b) SPOL, Melbourne, FL (i.e. R(Z,Zdr) vs. R(Z) for 21 events during July-Sept 1998).

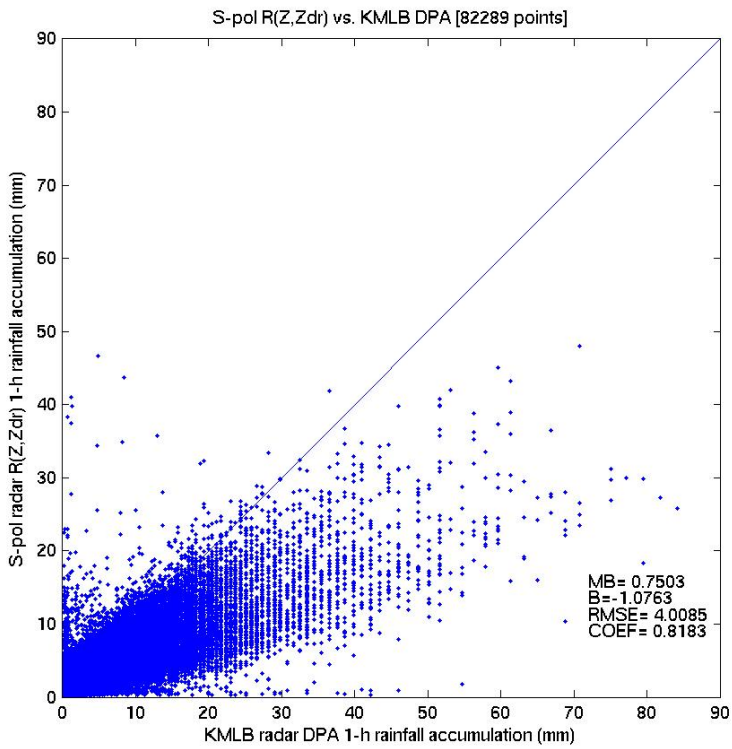

Fig. 2-2: Inter-radar (dual pol vs. horizontal pol) one-hour precipitation comparison for SPOL (i.e. R(Z,Zdr)) vs. KMLB (i.e. DPA product, derived from R(Z)), for 21 events during July-Sept 1998, Melbourne, FL. (Note: analogous to Fig. 2-1B, though dual pol SPOL R(Z,Zdr) now compared to single pol, operational WSR-88D DPA)

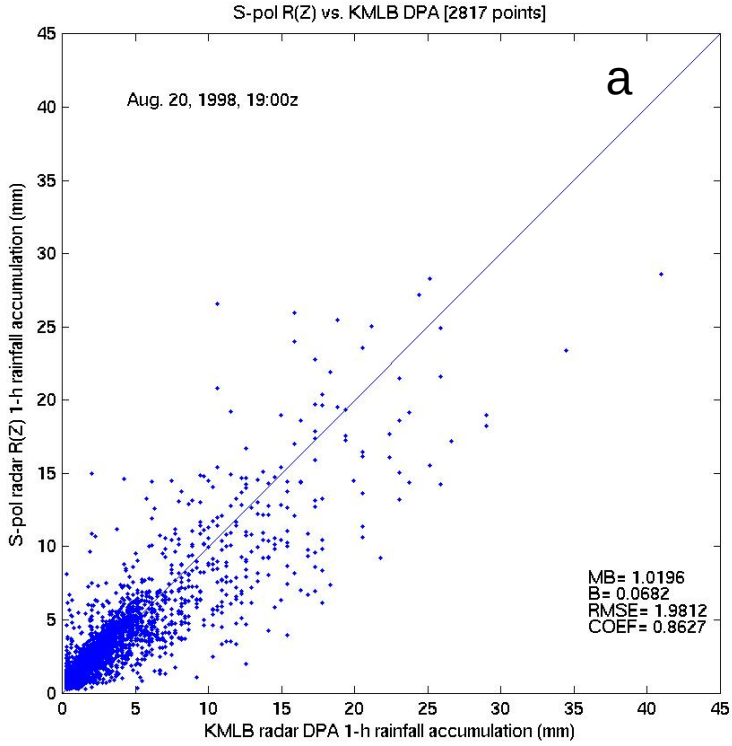

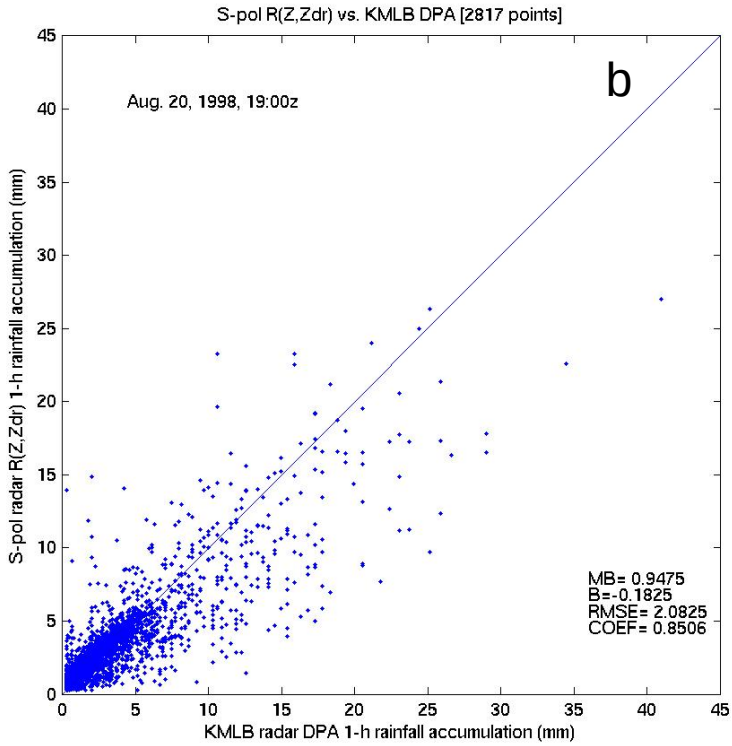

Fig. 2-3: Inter-radar precipitation comparisons of (a) SPOL R(Z) and (b) SPOL R(Z; Zdr), both against operational KMLB estimate for one hour period ending Aug. 20, 1998, 19:00z.

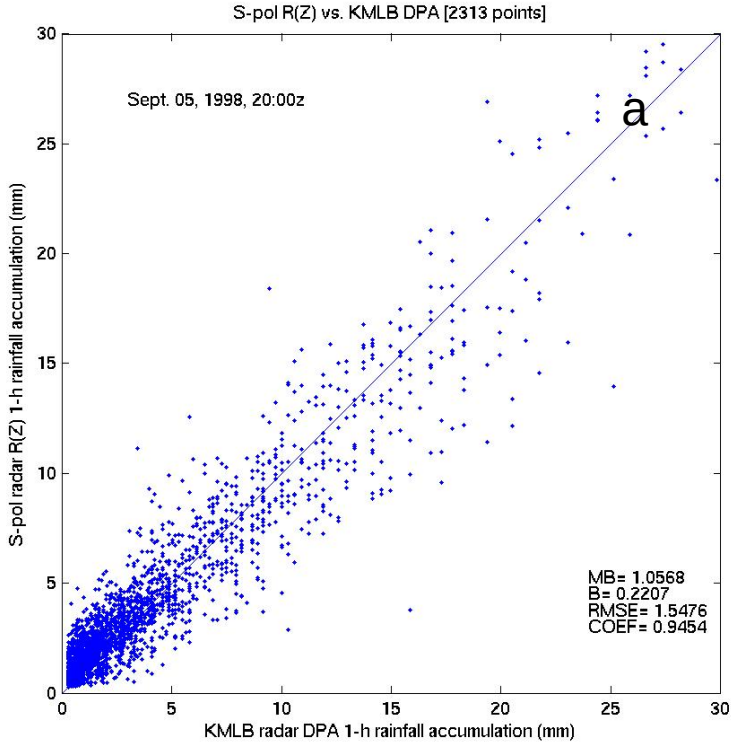

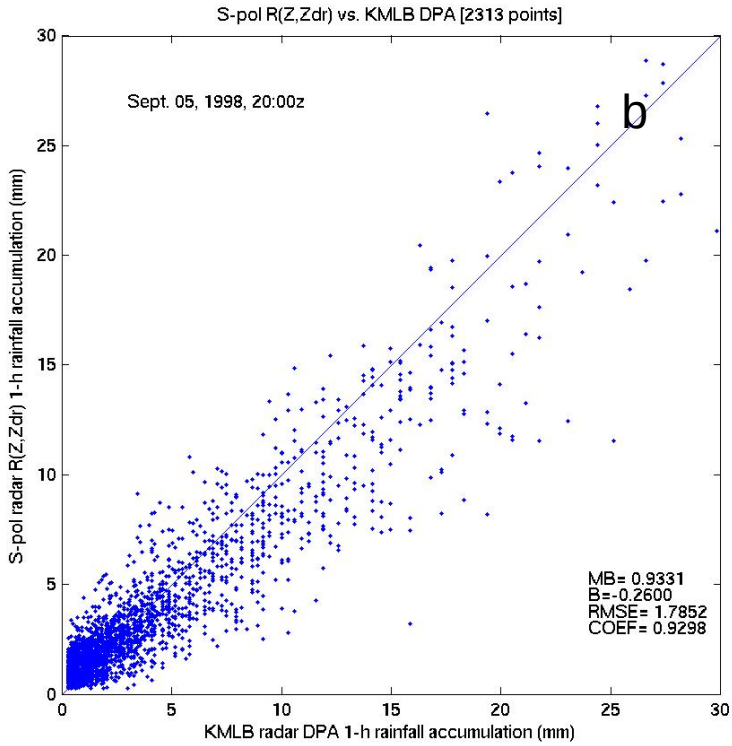

Fig. 2-4: Same as Fig. 2-3, for one hour period ending Sept. 05, 1998, 20:00z.

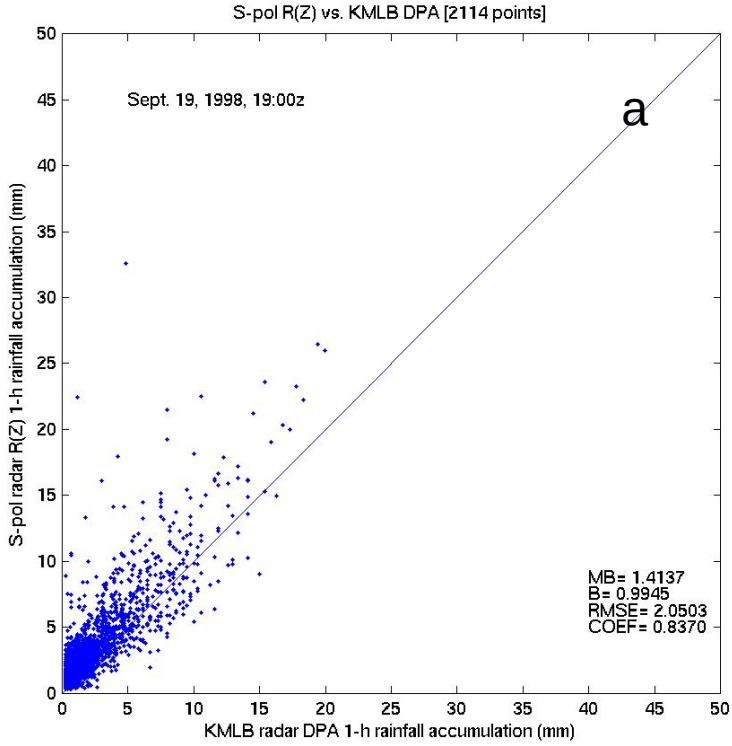

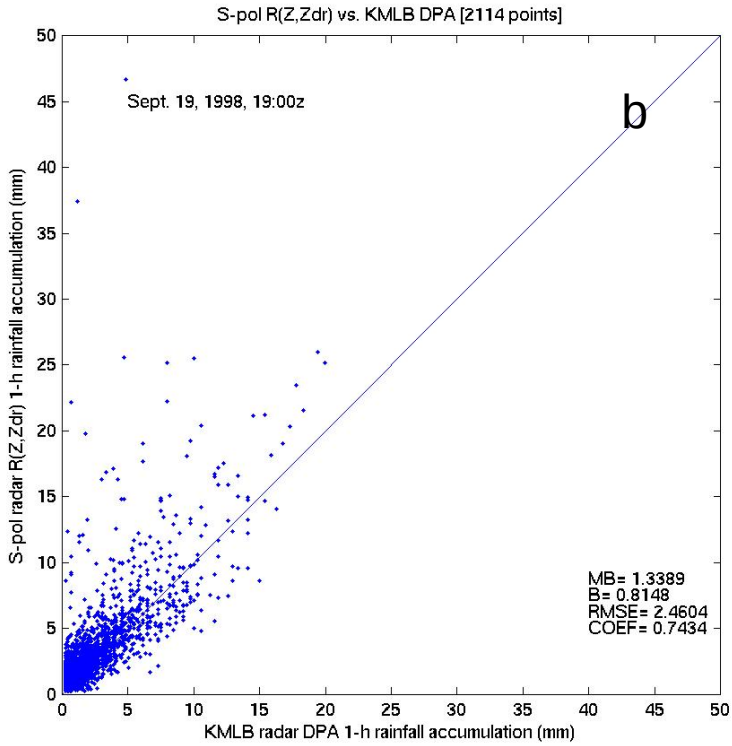

Fig. 2-5: Same as Fig. 2-3, for one hour period ending Sept. 19, 1998, 19:00z.

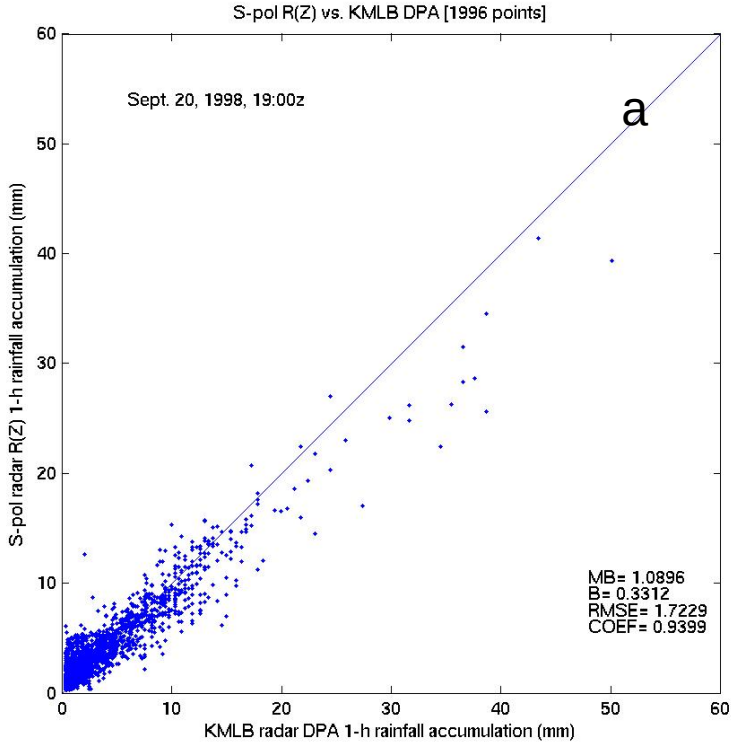

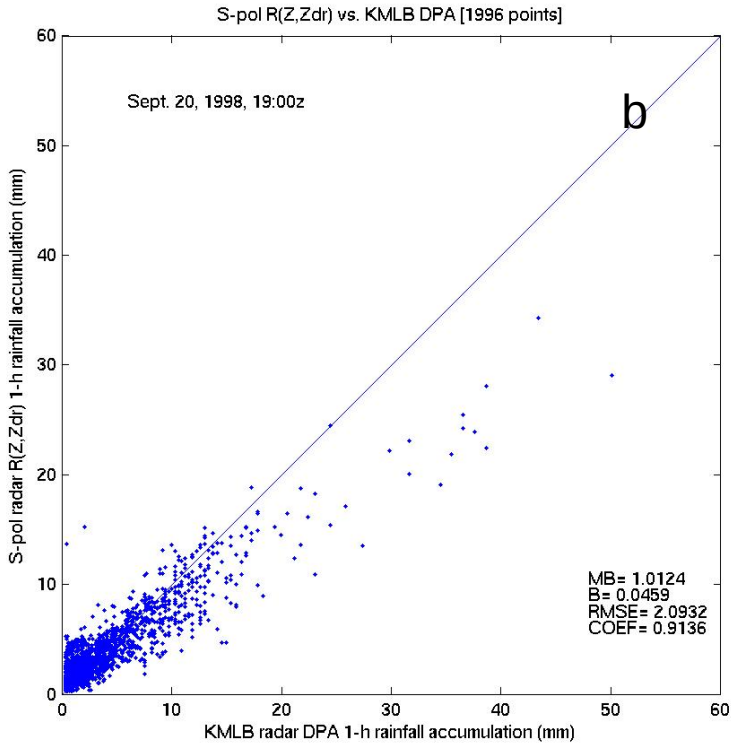

Fig. 2-6: Same as Fig. 2-3, for one hour period ending Sept. 20, 1998, 19:00z.

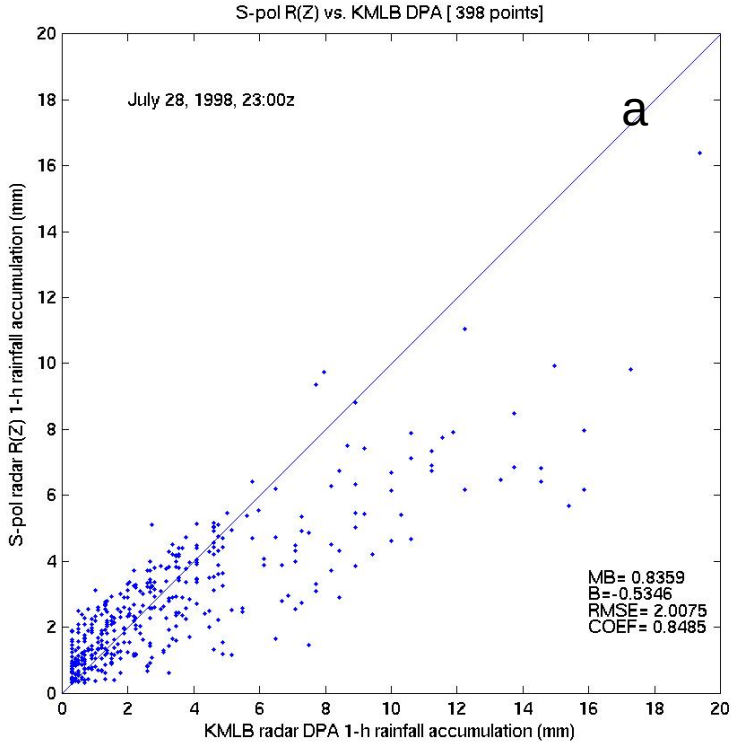

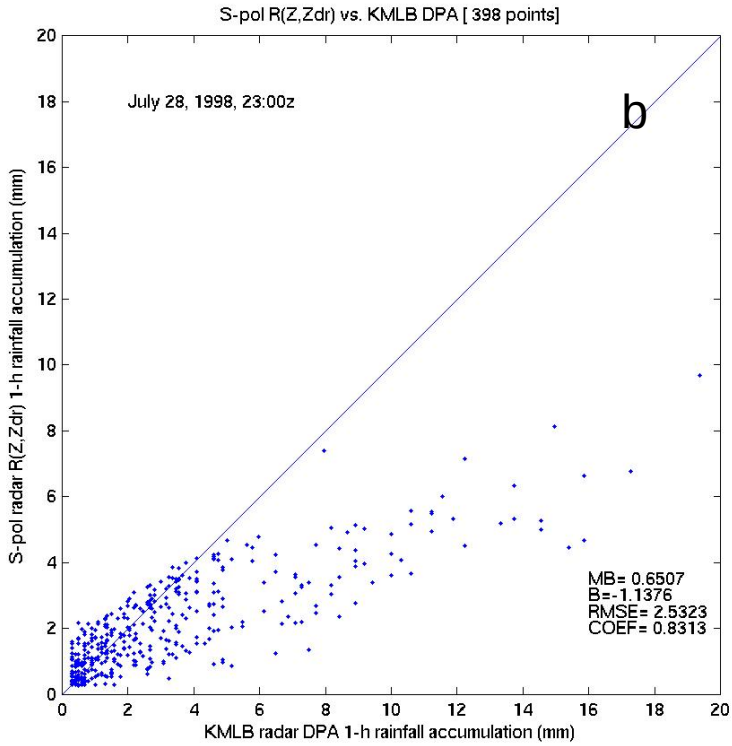

Fig. 2-7: Same as Fig. 2-3, for one hour period ending July 28, 1998, 23:00z.

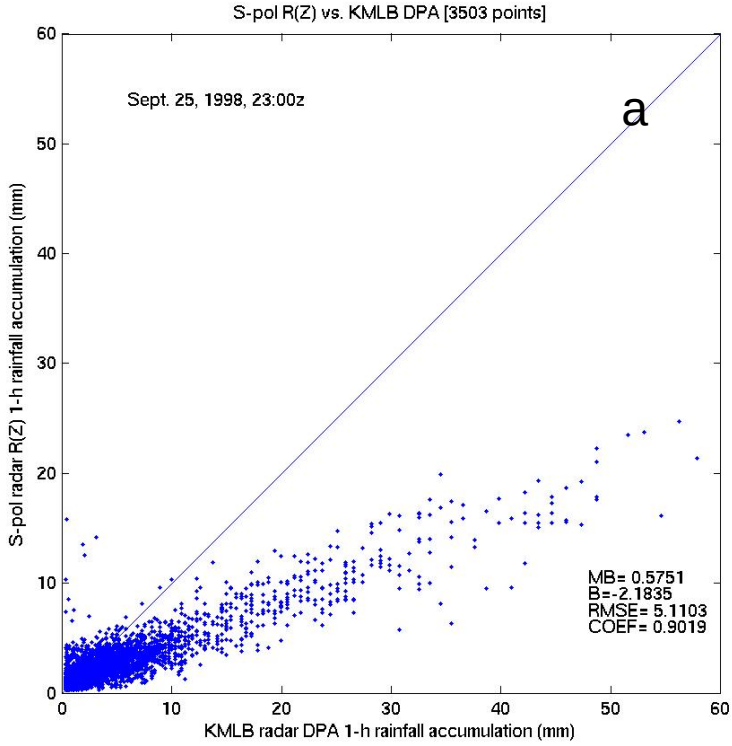

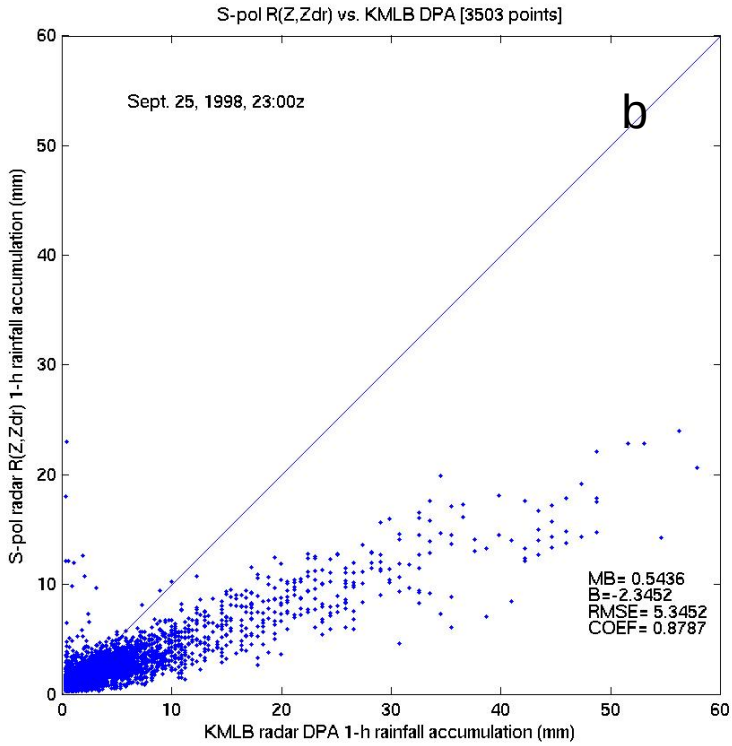

Fig. 2-8: Same as Fig. 2-3, for one hour period ending Sept. 25, 1998, 23:00z.

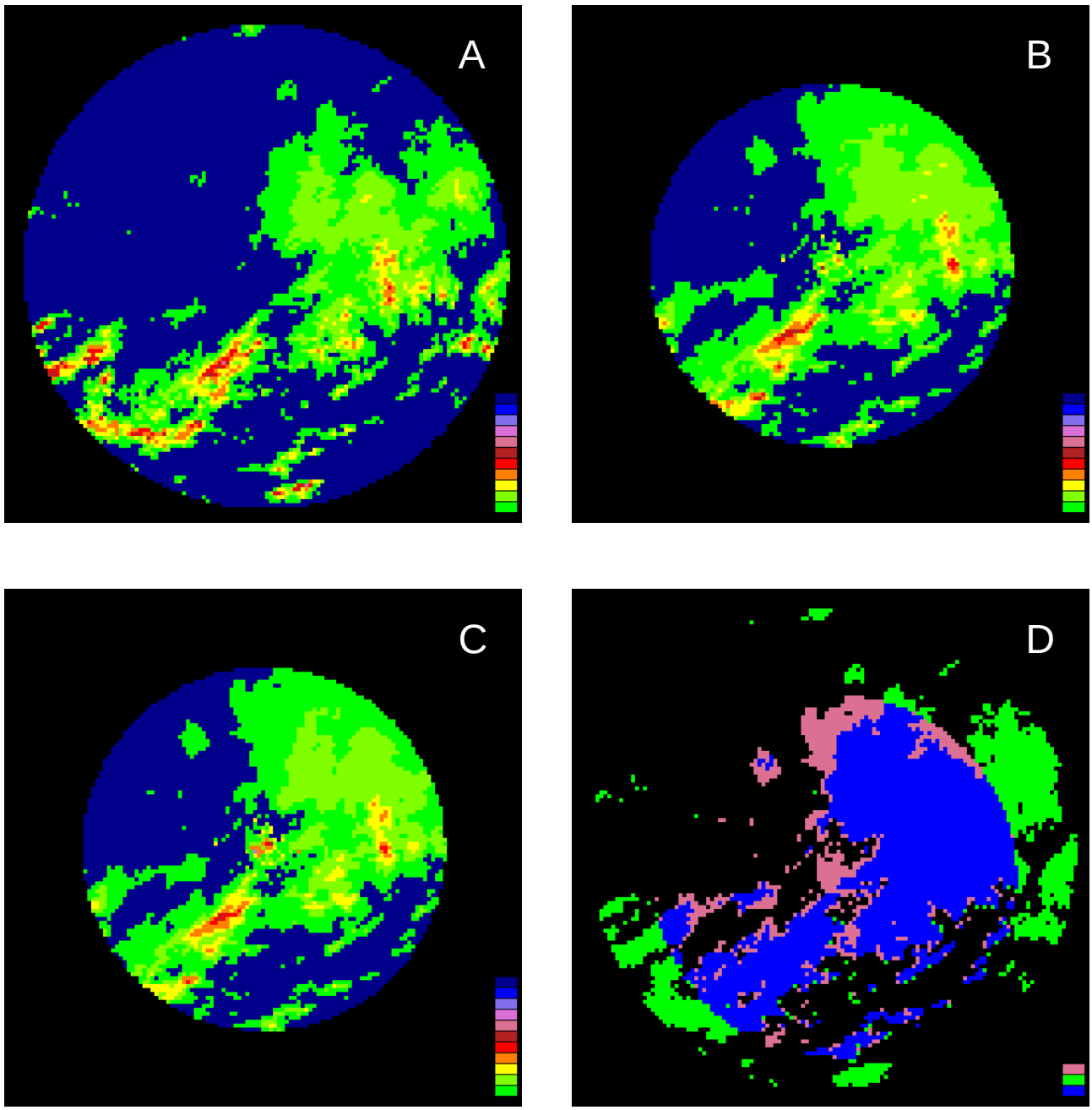

Fig. 2-9: One hour precip estimates from (A) KMLB DPA product; (B) SPOL radar, horizontal pol (R(Z)) algorithm; (C) SPOL radar, dual pol (R(Z;Zdr)) algorithm; and (D) comparison of A vs. C, for hour ending Aug. 20, 1998, 19:00z. Note: in (D) regions in green = only KMLB measurable precipitation; magenta = only SPOL measurable precipitation; blue = both.

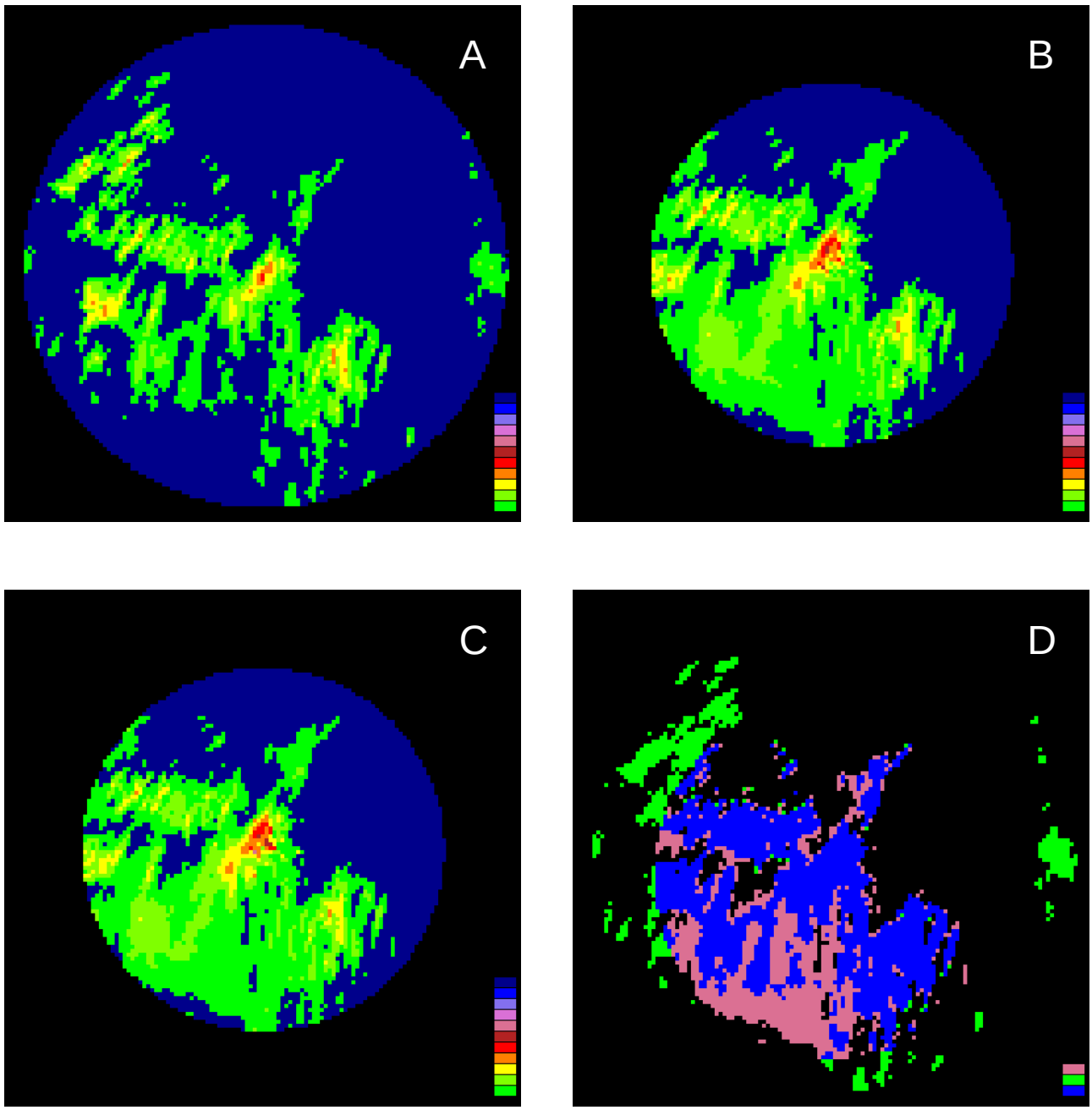

Fig. 2-10: Same as Fig. 2-9, for hour ending Sept. 19, 1998, 19:00z.

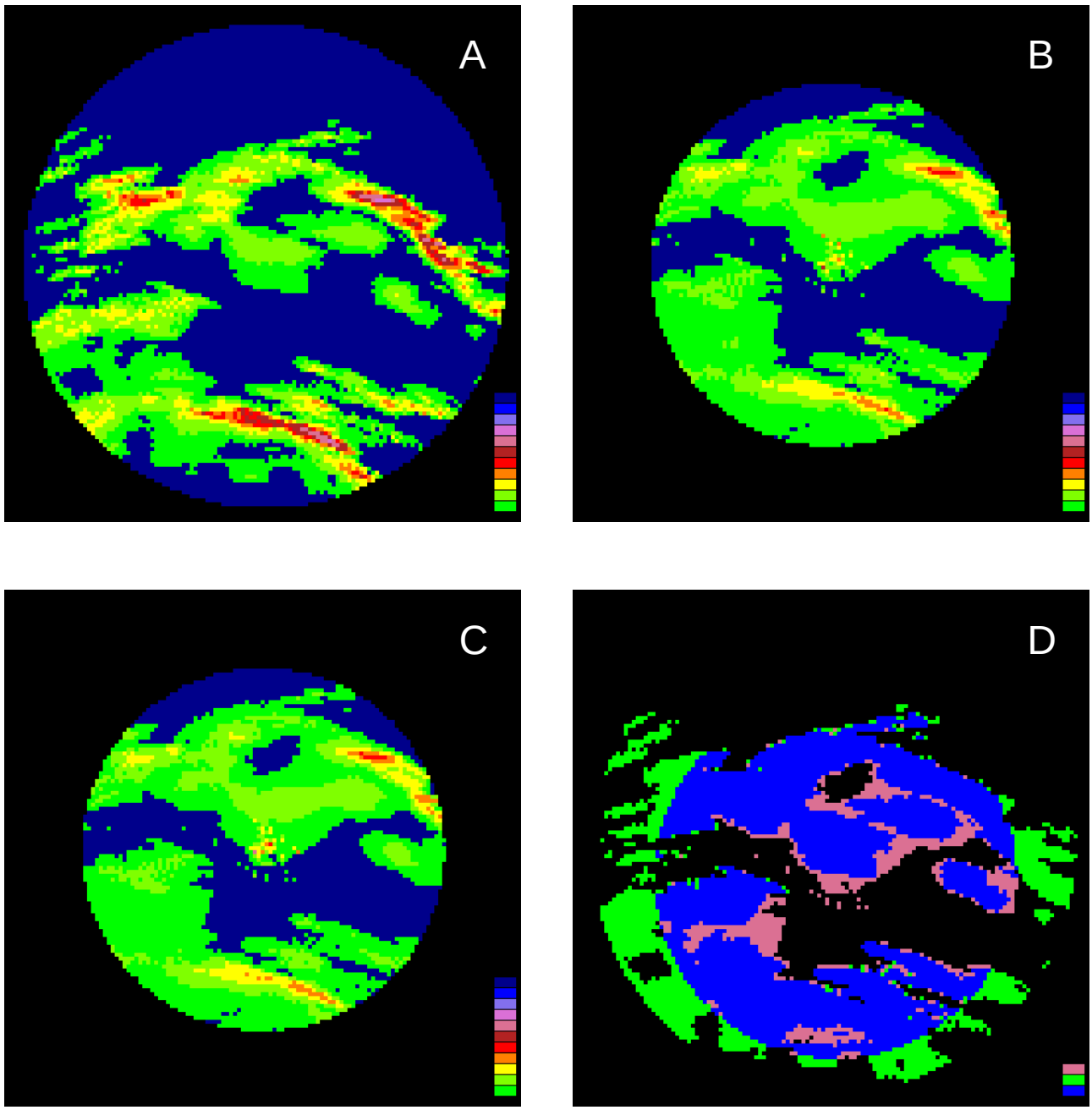

Fig. 2-11: Same as Fig. 2-9, for hour ending Sept. 25, 1998, 23:00z.

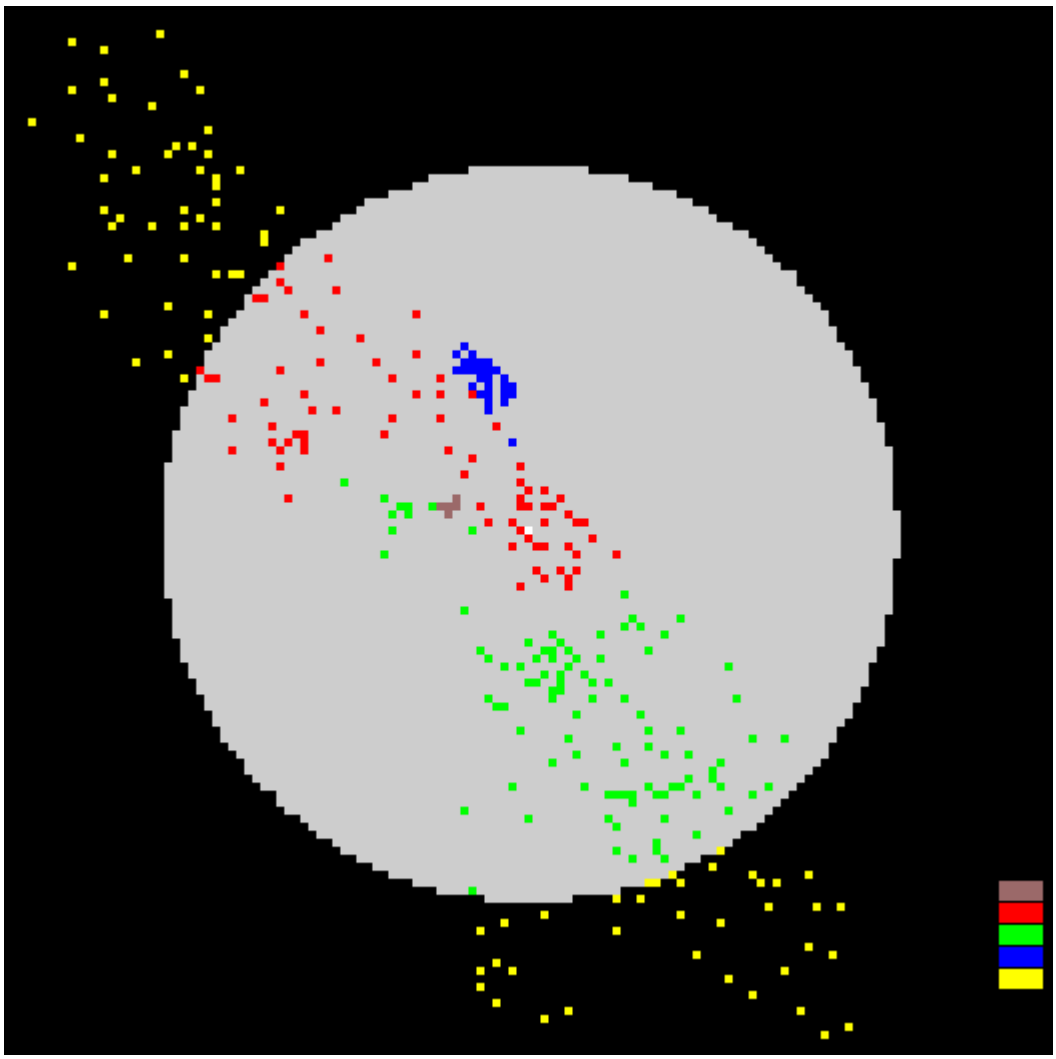

Fig. 2-12: Locations of all TRMM-GV gages. Note: only those gages within the coverage area of the SPOL radar (gray) were used in this study.

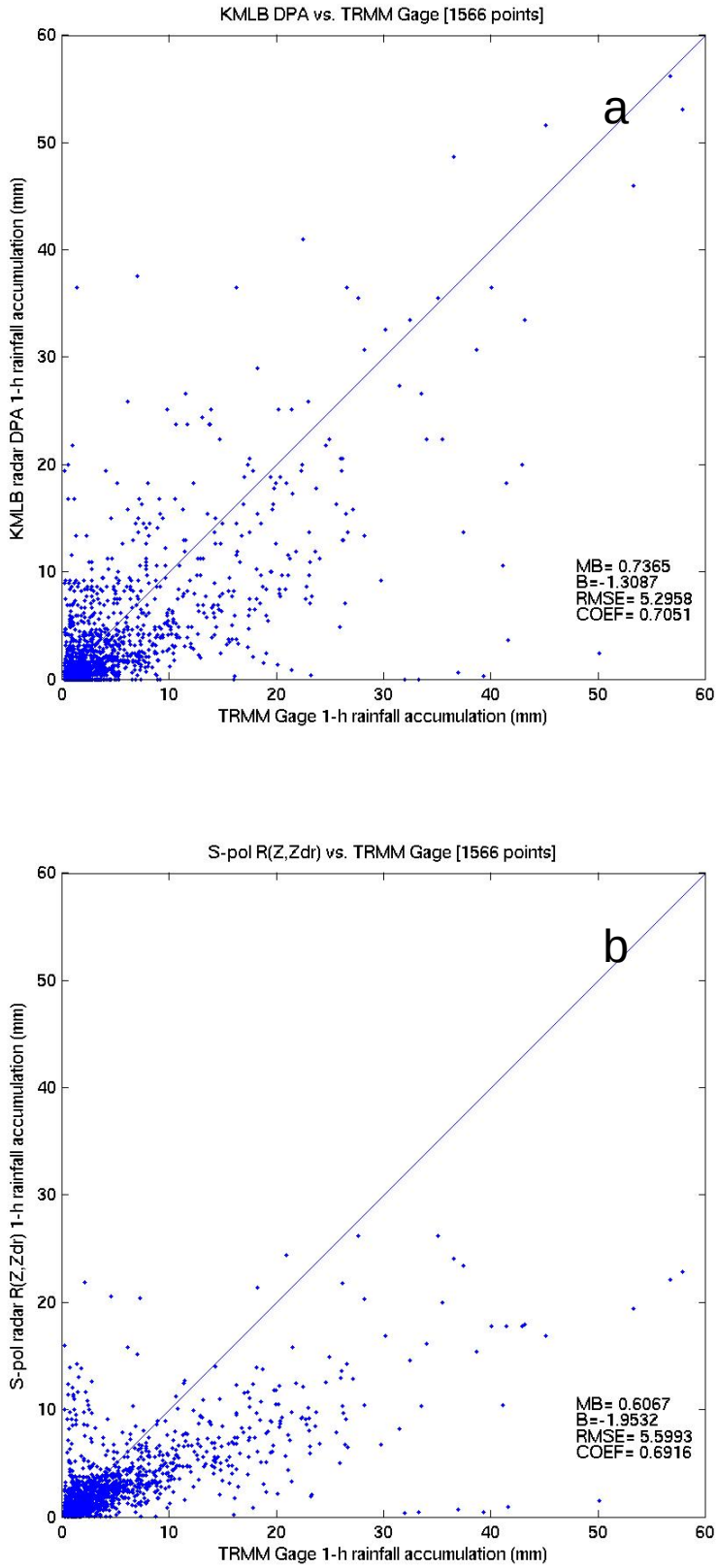

Fig. 2-13: Radar vs. rain gage precipitation comparisons from: (A) KMLB DPA product; and (B) SPOL R(Z; Zdr) estimate, both against TRMM-GV one-hour gage reports, for all events in the period July 28-Sept. 26, 1998.

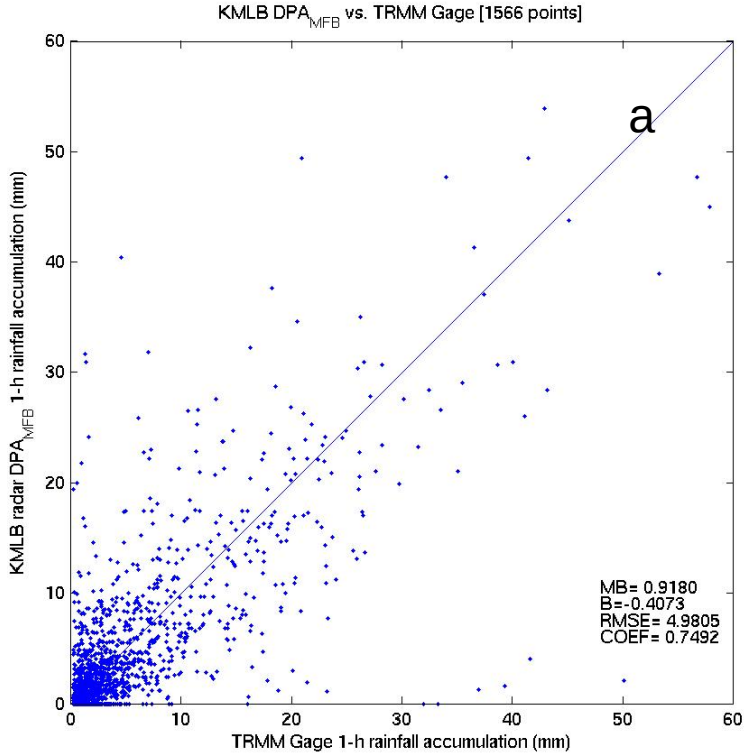

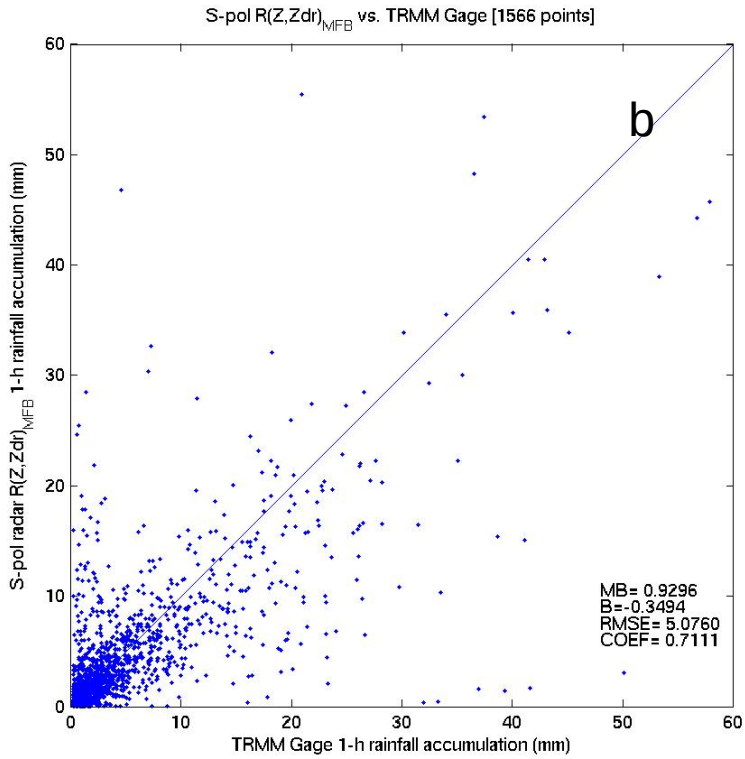

Fig. 2-14: Same as Fig. 2-13, after MFB correction applied to radar estimates.

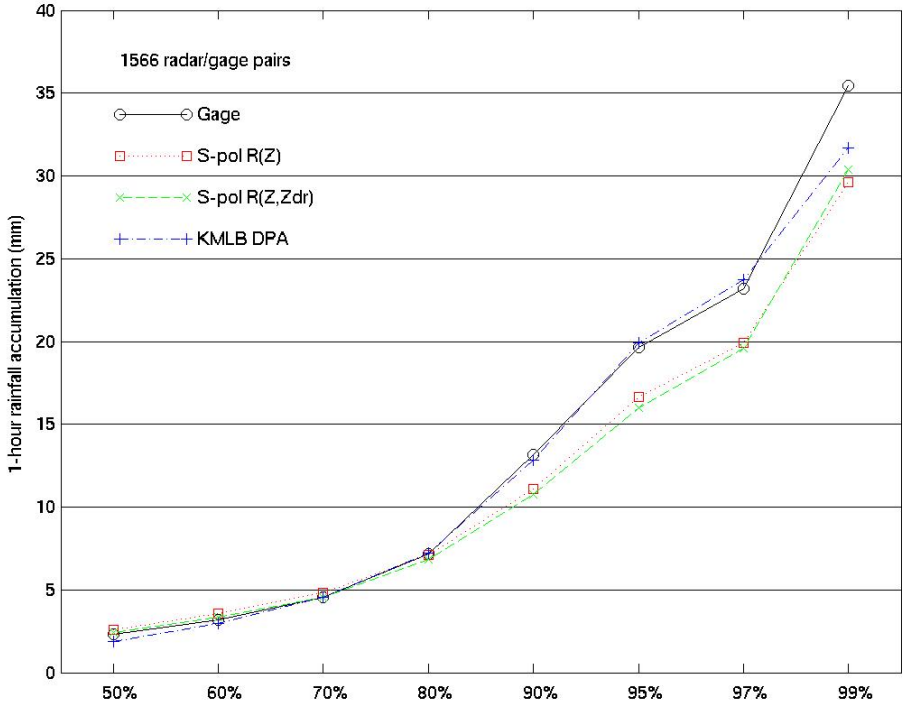

Fig. 2-15: Percentile breakdown of hourly rainfall estimates from TRMM-GV gages (solid trace); SPOL R(Z); SPOL R(Z,Zdr); and KMLB DPA.

Task 1.2: Potential Applications Of NSSL Dual-Polarization Hydrometeor Classifier Algorithm (HCA) As A Precipitation/No Precipitation Filter

A need currently exists for better identification and removal of nonprecipitation features from the radar estimates currently supplied to River Forecast Centers (RFCs). Particularly during the spring and autumn bird migrations, extensive areas identified as light precipitation appear in circular regions roughly concentric about radar sites. On occasion, return from insects is also high enough to cause anomalous light precipitation accumulations. The evolving WSR-88D dual-polarization quantitative precipitation estimation (DP-QPE) (Ryzhkov et al. 2005a,b) algorithm and Hydrometeor Classification Algorithm (HCA) (Ryzhkov et al. 2005a) could mitigate this problem. The examples shown below demonstrate the ability of HCA to identify and eliminate anomalous rainfall from estimates of the KOUN dual-polarization prototype unit, in cases where the nearby KTLX WSR-88D showed extensive light anomalous precipitation.

Note that this analysis used version 1 of the NSSL's DP-QPE algorithm and HCA, hereafter designated Combined and HCA1, respectively. Although we only considered QPE1 and HCA1 in this analysis, work on a newer version with the same benefits is underway (Ryzhkov, personal communication). The rainfall estimates themselves are from QPE1, but we are not considering the precision of the estimates themselves, only the representation of the rainfall pattern.

It appears that the HCA1 successfully identifies biota and eliminates anomalous reflectivity features associated with them. An opportunity exists to either apply the HCA1 directly to horizontal polarization rainrate estimates, or to apply dual-pol QPE itself as a mask to eliminate areas of spurious precipitation. To examine the latter possibility, we identified several cases in which operational QPEs from the KTLX WSR-88D unit appeared to have both true precipitation and anomalous accumulations from biota. The dual-pol Combined fields were then examined to determine if those areas with anomalous accumulations were eliminated. Though this evaluation is partly subjective, we included rain gauge reports from the Oklahoma Mesonet as an additional form of ground truth.

A combination of precipitation- and biota-based accumulations over Oklahoma during the early morning hours of 13 May 2005 is shown in Figs. 3-1,2. In both figures, data in (a) are from operational KTLX One Hour Precipitation products, overlaid on Mesonet gauge reports. Note that the maximum range of the estimates is slightly greater for the KOUN dual-pol estimates, 250 km vs. 230 km for KTLX.

In Figs. 3-1,2, a large area of echoes concentric on the radar site led to light precipitation accumulations in both images, while a mesoscale convective complex approaches from the west. The zero gauge reports clearly identify the area near the radar as anomalous precipitation, probably from a combination of migrating birds and insects. The KOUN representation of the convective complex in (b) closely resembles that of the KTLX unit, while only some small areas of clutter-induced anomalous precipitation appears near the

KOUN radar itself. Clutter suppression was generally not available for the KOUN data processing suite.

Similar results held for the case of 30 May 2004, shown in Fig. 3-3, where an isolated intense storm cells near the two radar units was embedded in an area of biota return.

We noted that in both cases, some lighter, probably high-altitude, precipitation appeared at longer ranges in the KTLX data but not in the KOUN estimates. In all cases coincident gauge reports were zero. While these accumulations appear to be hydrometeors, it is possible that the HCA1 indicated only an ambiguous classification and thus the area was dropped from accumulations. The lack of reported surface rain could be due to subcloud evaporation. We did note that the HCA1 did not appear to miss any gauge-reported precipitation.

Depending on the results of further analysis, we will propose that end-users be given the option of using the DP-QPE1 precipitation accumulations as a quality-control mask as soon as the product is available. Such a mask utility could be applied within AWIPS through the D2D and MPE packages, to accumulations from the existing WSR-88D precipitation processing system, or to estimates from radars.

Acknowledgements

Dual-polarization QPE1 fields were supplied by John Krause and Alexander Ryzhkov of NSSL. Rain gauge reports were supplied by the Oklahoma Climate Survey.

References

Ryzhkov, A. V., T. J. Schuur, D. W. Burgess, P. L. Heinselman, S. E. Giangrande, and D. S. Zrnic, 2005a: The Joint Polarization Experiment: Polarimetric rainfall measurements and hydrometeor classification. *Bull. Amer. Meteor. Soc.*, **86**, 809-824.

Ryzhkov, A. V., S. E. Giangrande, T. J. Schuur, 2005b: Rainfall Estimation with a Polarimetric Prototype of WSR-88D. *J. Appl. Meteor.*, **44**, 502-515.

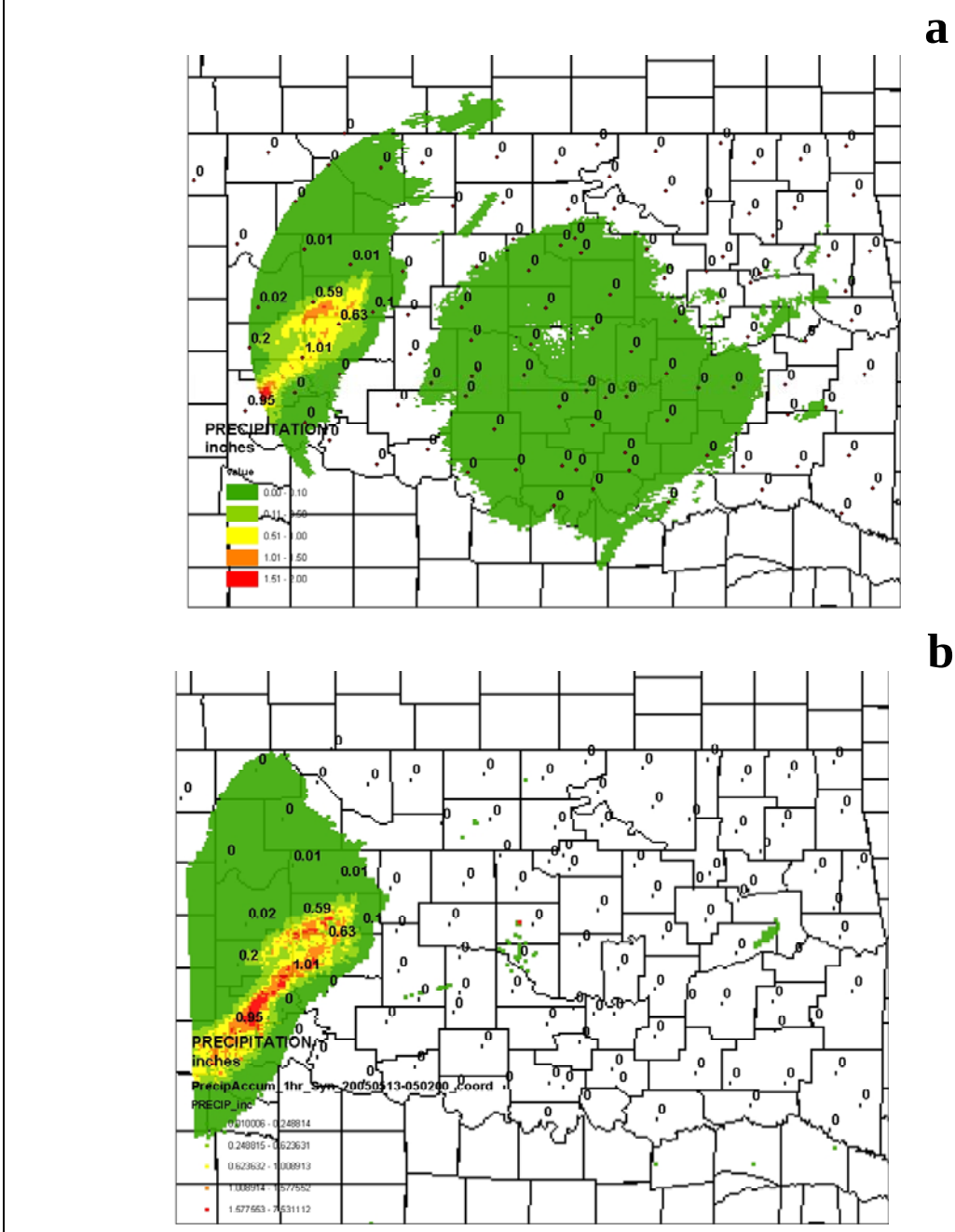

Figure 3-1. One-hour precipitation ending 0500 UTC, 13 May 2005, from (a) WSR-88D KTLX (OHP) and (b) KOUN "Synthetic" dual-pol algorithm, incorporating Hydrometeor Classification Algorithm Version 1. Rain gauge reports in inches are shown in (a).

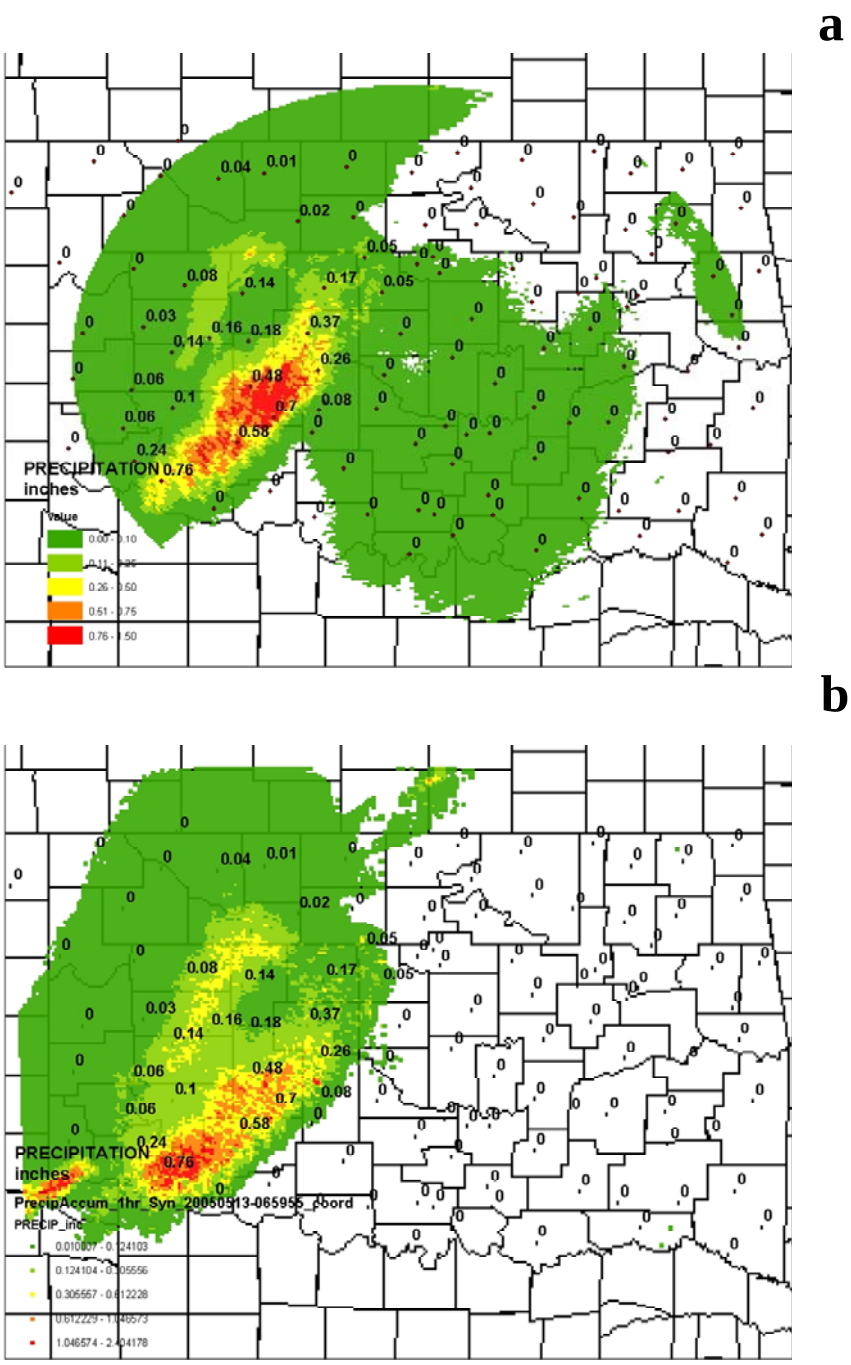

Figure 3-2. As in Fig. 1, except for 0700 UTC, 13 May 2005.

a

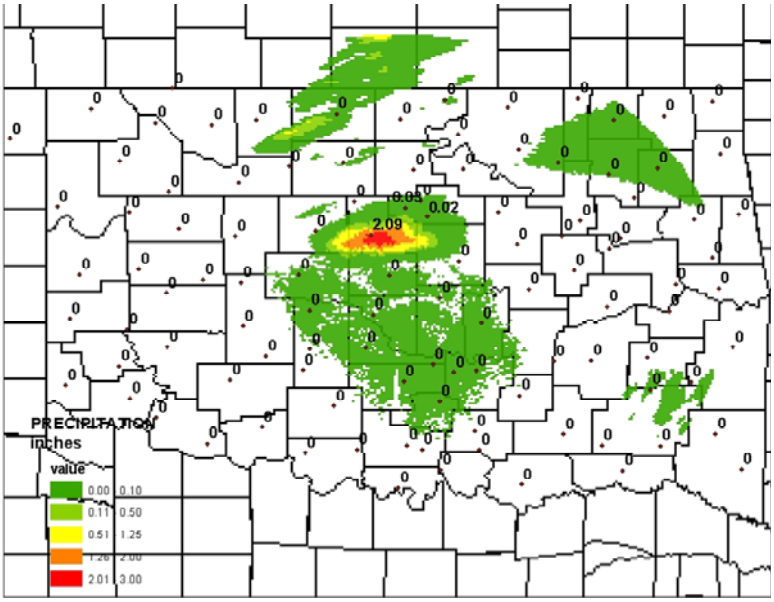

b

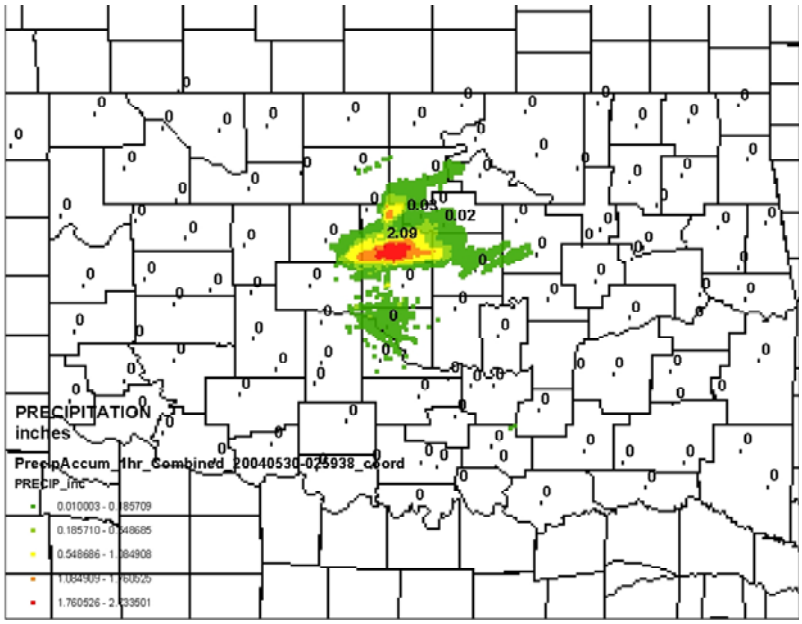

Figure 3-3. As in Fig. 1, except for 0300 UTC, 30 May 2004.